# Structural Basis for Tailor-Made Modulation of G Protein Coupled Receptor Functionality

Dissertation zur Erlangung des akademischen Grades
des Doktors der Naturwissenschaften (Dr. rer. nat.)

eingereicht im Fachbereich Biologie, Chemie, Pharmazie
der Freien Universität Berlin

vorgelegt von
**Marcel Bermudez Sasso**
aus Schönebeck
2015

Die vorliegende Arbeit wurde von Februar 2011 bis April 2015 unter der Leitung von Prof. Dr. Gerhard Wolber am Institut für Pharmazie der Freien Universität Berlin angefertigt.

1. Gutachter: Prof. Dr. Gerhard Wolber
2. Gutachter: Prof. Dr. Ingo Ott

Disputation am: 16.06.2015

# Acknowledgements

The present work was carried out at the Institute of Pharmacy of the Freie Universität Berlin from 2011 to 2015.

In the first place, I would like to thank Prof. Dr. Gerhard Wolber for the nice and friendly supervision during the last years. Secondly, I would like to thank all my colleagues at the computer-aided drug design lab for the nice working atmosphere, especially in the room 276. A special thank goes to Christin Rakers for her support in analyzing MD simulations.

I would also like to thank all collaboration partners that provided invaluable information and data in this highly interdisciplinary field of research: the lab of Prof. Dr. Ulrike Holzgrabe in Würzburg, the group of Prof. Dr. Klaus Mohr in Bonn, Prof. Dr. Thomas Wieland and his working group in Heidelberg and Andreas Bock from Würzburg.

I like to thank the computing center of the FU Berlin (ZEDAT) for providing the compute cluster SOROBAN for molecular dynamics simulations.

Finally, I would not have come so far without the unresting support of my family. Therefore, I want to thank my parents, my sister and especially Elena.

# Table of Contents

# List of Abbreviations

| | | |
|---|---|---|
| 2D | = | two-dimensional |
| 3D | = | three-dimensional |
| AC | = | Adenylate cyclase |
| ACh | = | Acetylcholine |
| AChE | = | Acetylcholine esterase |
| AD | = | Alzheimer's disease |
| cAMP | = | Cyclic adenosine monophosphate |
| cGMP | = | Cyclic guanosine monophosphate |
| CNS | = | Central nervous system |
| COPD | = | Chronic obstructive pulmonary disease |
| CPU | = | Central processor unit |
| DAG | = | Diacylglycerol |
| DRY | = | Asp-Arg-Tyr |
| EDGE | = | Glu-Asp-Gly-Glu |
| EL2 | = | Extracellular loop 2 |
| EL3 | = | Extracellular loop 3 |
| GDP | = | Guanosine diphosphate |
| GTP | = | Guanosine triphosphate |
| GPCR | = | G protein-coupled receptor |
| HM | = | Homology model |

| | | |
|---|---|---|
| IL3 | = | Intracellular loop 3 |
| IP3 | = | Inositol trisphosphate |
| MAChR | = | Muscarinic acetylcholine receptor |
| Mx AChR | = | Subtype x muscarinic acetylcholine receptor |
| MD | = | Molecular dynamics |
| NPxxY | = | Asn-Pro-x-x-Tyr |
| OBP | = | Orthosteric binding pocket |
| OTC | = | Over-the-counter |
| PDB | = | Protein data bank |
| PLC | = | Phospholipase C |
| PKC | = | Protein kinase C |
| POPC | = | Palmitoyl-oleoyl-phosphatidyl-choline |
| Rac1 | = | Ras-related C3 botulinum toxin substrate |
| RMSD | = | Root-mean-square deviation |
| TM | = | Transmembrane domain |
| 7TM | = | Seven transmembrane receptors |

# 1 Introduction

G protein coupled receptors (GPCRs) belong to the family of seven-transmembrane domain proteins. They are expressed in nearly all kinds of tissues and contribute to the regulation of an enormous variety of physiological functions [1]. To fully utilize the therapeutic potential of GPCRs, detailed knowledge about structural and functional properties is required. The following sections will give an overview about GPCRs, their classification schemes, their structural features and the associated signaling repertoire representing the most relevant property for their therapeutic relevance.

## 1.1 Classification of GPCRs and their ligands

The human genome contains over 800 genes coding for functional GPCRs. Based on their primary sequence, these genes were historically classified into three main families: A, B, C or 1, 2, 3, respectively [2]. Class A represents the largest group and contains the rhodopsin-like receptors - interestingly most of them are olfactory receptors [3]. In the scientific literature, class A and rhodopsin-like receptors are often used as synonyms. Several alternative classification systems were established, for example the A-F classification by Kolakowski [4] or the differentiation on the basis of structure and ligand-binding criteria [5].

Later, the *GRAFS* classification system was established (Figure 1), which subdivides GPCRs into five main families according to their phylogenetic distance, named *Glutamate*, *Rhodopsin*, *Adhesion*, *Frizzled/Taste2*, and *Secretin* [6]. Surprisingly, there is no connection between the phylogenetic group of a receptor and the type of endogenous ligand [7]. The largest family are rhodopsin-type GPCRs being subdivided into four main groups termed α, β, γ and δ with 13 sub-branches [8]. Muscarinic acetylcholine receptors (MAChRs), which the presented thesis is focusing on, belong to the α group of the *Rhodopsin* family and are further sub-divided into five subtypes ($M_1$-$M_5$ MAChR).

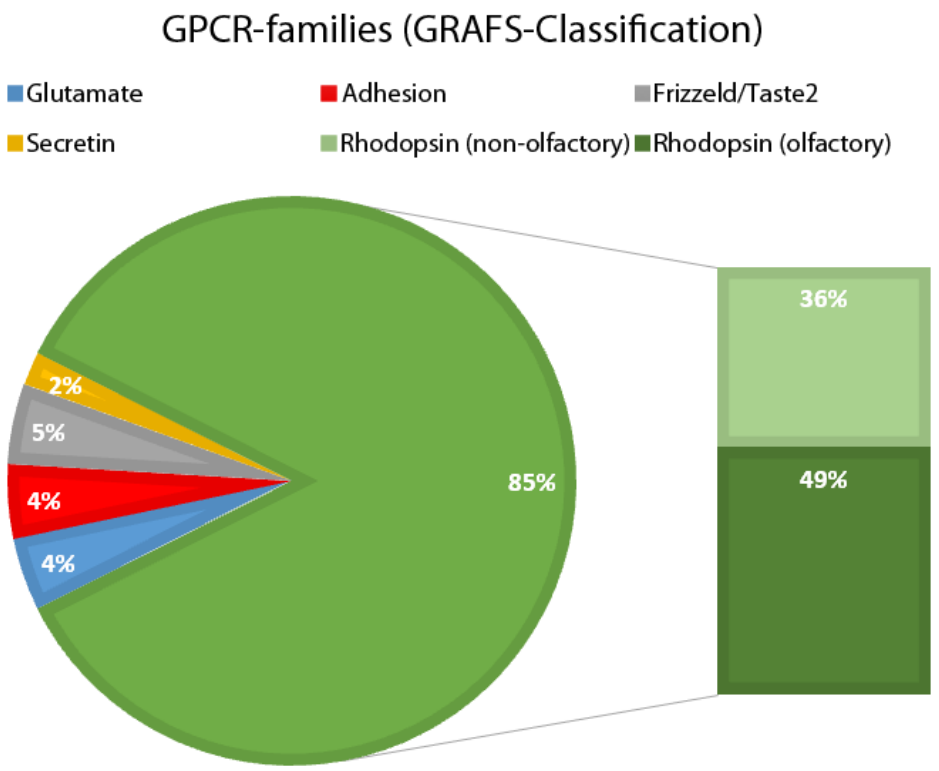


Figure 1: Overview of GPCR families. Most GPCRs are classified in the *Rhodopsin* family (672) although most of them are olfactory receptors (388) [3]. The other GPCRs are distributed almost equally among the *Glutamate* (22), *Adhesion* (33), *Frizzeld/Taste2* (36) and the *Secretin* family (15).

In contrast to the receptors themselves, the classification of GPCR ligands represents a much more complex challenge: Ligands can be categorized according to their influence on the receptor function or on the location of their binding site that can be either orthosteric or allosteric [9]. Most GPCRs are constitutively active, which results in a basal signaling activity [10]. Depending on the influence on this basal activity, ligands can be classified as agonists, inverse agonists or antagonists depending on whether they increase, decrease or do not influence the basal activity [11]. Agonists are further characterized by their ability to induce receptor activation. A full agonist (e.g. a physiological activator) binds to the receptor with high affinity and stabilizes the active receptor conformation, whereas a partial agonist only induces submaximal receptor activation [12]. Superagonists have a higher efficacy for receptor activation than the physiological agonist [13]. Endogenous ligands as well as therapeutically used agonists, inverse agonists and antagonists typically occupy the orthosteric binding site that shows high conservation between single receptor subtypes [9] (Figure 2).

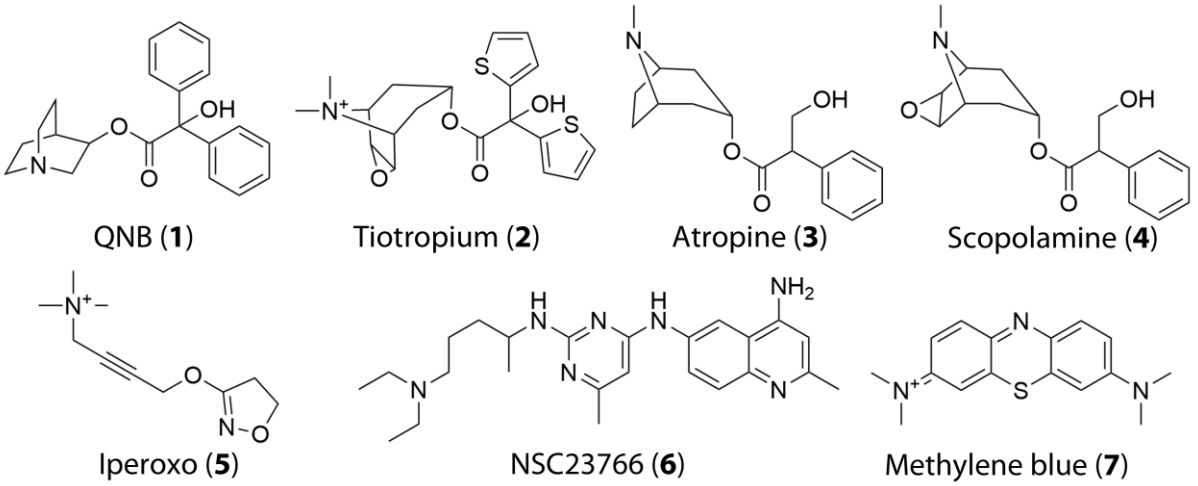


Figure 2: 2D representations of orthosteric MAChR ligands.

However, ligand binding is not restricted to the orthosteric binding site: Allosteric ligands (Figure 3) can influence the binding of orthosteric ligands by allosteric modulation [12]. These can be classified as positive or negative allosteric modulators, if they enhance or decrease the binding of orthosteric ligands, respectively [14]. Furthermore, allosteric binders can change the receptor activation state themselves.

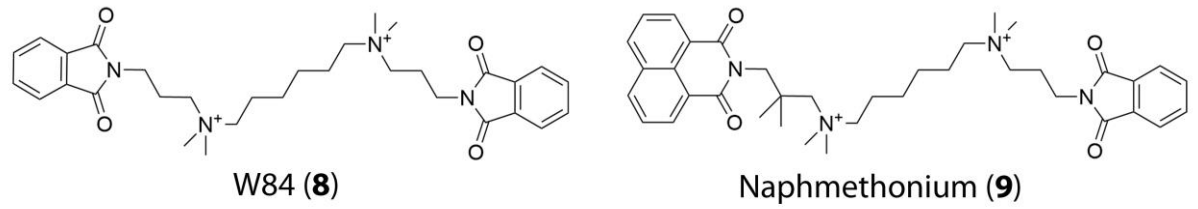


Figure 3: 2D representations of allosteric MAChR ligands.

A bitopic ligand is defined to bind at two locations (e.g. binds to two different receptors or bridge two neighboring receptors) [15]. A special case of bitopic binding is a ligand that binds simultaneously to two different binding sites (orthosteric/allosteric) at the same receptor, which is called *dualsteric ligand binding*. Depending on their orthosteric building block they can be classified as dualsteric antagonists (Figure 4) or dualsteric agonists (Figure 5).

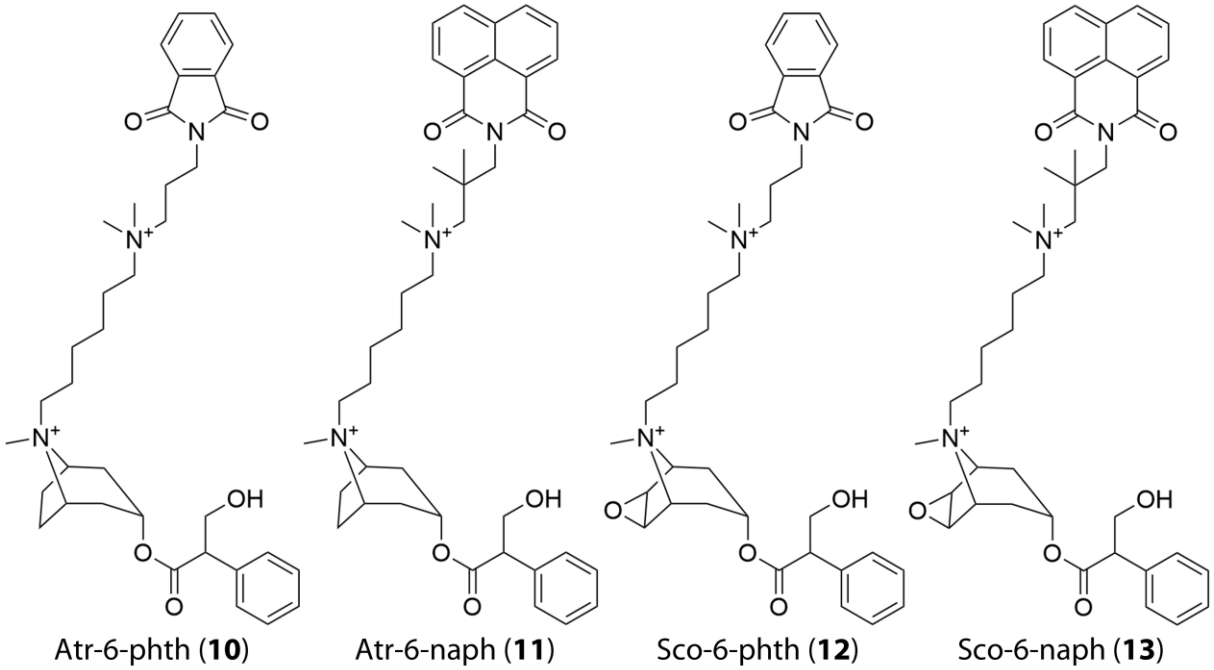


Figure 4: 2D representations of investigated dualsteric MAChR antagonists.

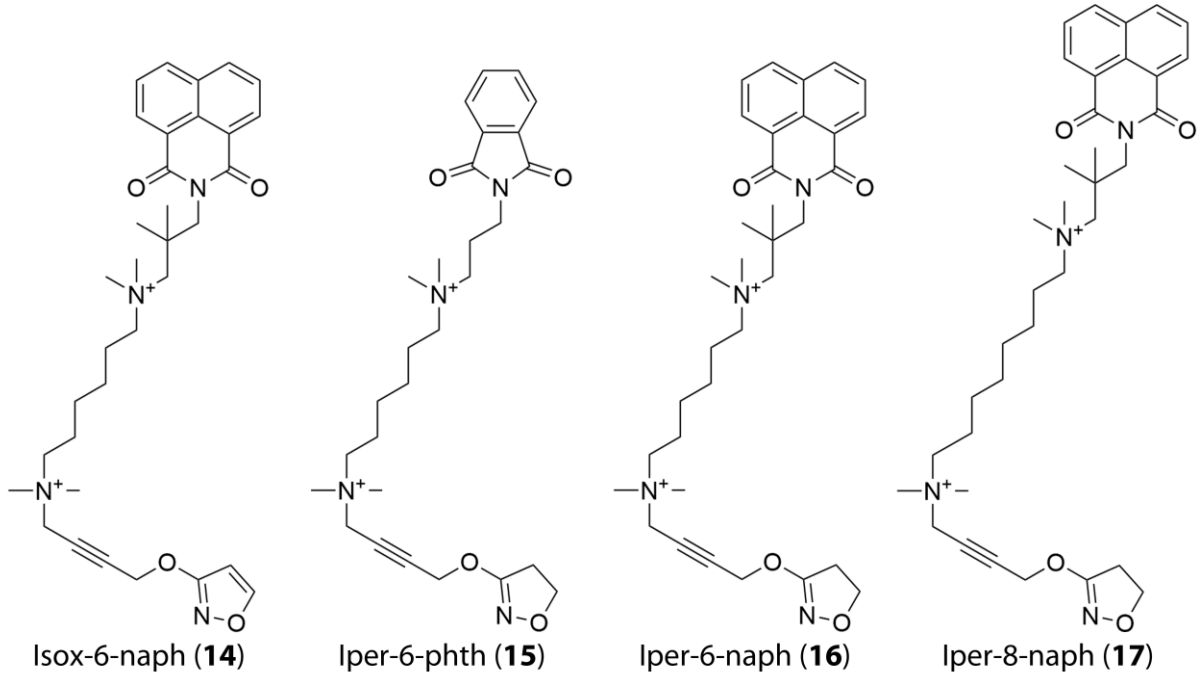


Figure 5: 2D representations of investigated dualsteric MAChR agonists.

Due to multiple signaling pathways resulting from receptor activation [16], the ligand classification can differ for one and the same ligand regarding different intracellular signaling pathways, which renders a consistent ligand classification impossible.

## 1.2 Structure of GPCRs

Besides their property to trigger G protein release, GPCRs can also be referred to as seven-transmembrane receptors (7TM), which describes their overall architecture of seven helices that are embedded in the membrane. The term 7TM receptors reflects that signaling mechanisms are not restricted to G protein binding [17] (see also chapter 1.4).

A common structural property of GPCRs is the serpentine transmembrane topology, which is composed of seven alpha-helical domains that are connected by intra-and extracellular loops of variable structure (Figure 6).

The evolutionary success of GPCRs is based on the possibility to expand, specialize and fine-tune biological communication and therefore requires high structural diversity [7]. Especially the extracellular loop 2 (EL2) shows high variability and can either form helical segments (e.g.: $\beta_2$ adrenoceptor) or also β- sheets (e.g.: rhodopsin) [18]. The N-terminus is located extracellularly and the C-terminal tail is anchored to the intracellular face of the lipid bilayer via palmitoylation to produce a short intracellular loop, which typically forms an alpha-helical structure (helix8) [19]. A closer look at the protein sequence unveils highly conserved motifs that are essential for receptor function [20]: These include the DRY(Asp-Arg-Tyr) motif at the end of TM3 or the NPxxY motif (Asn-Pro-x-x-Tyr) [19, 21, 22].

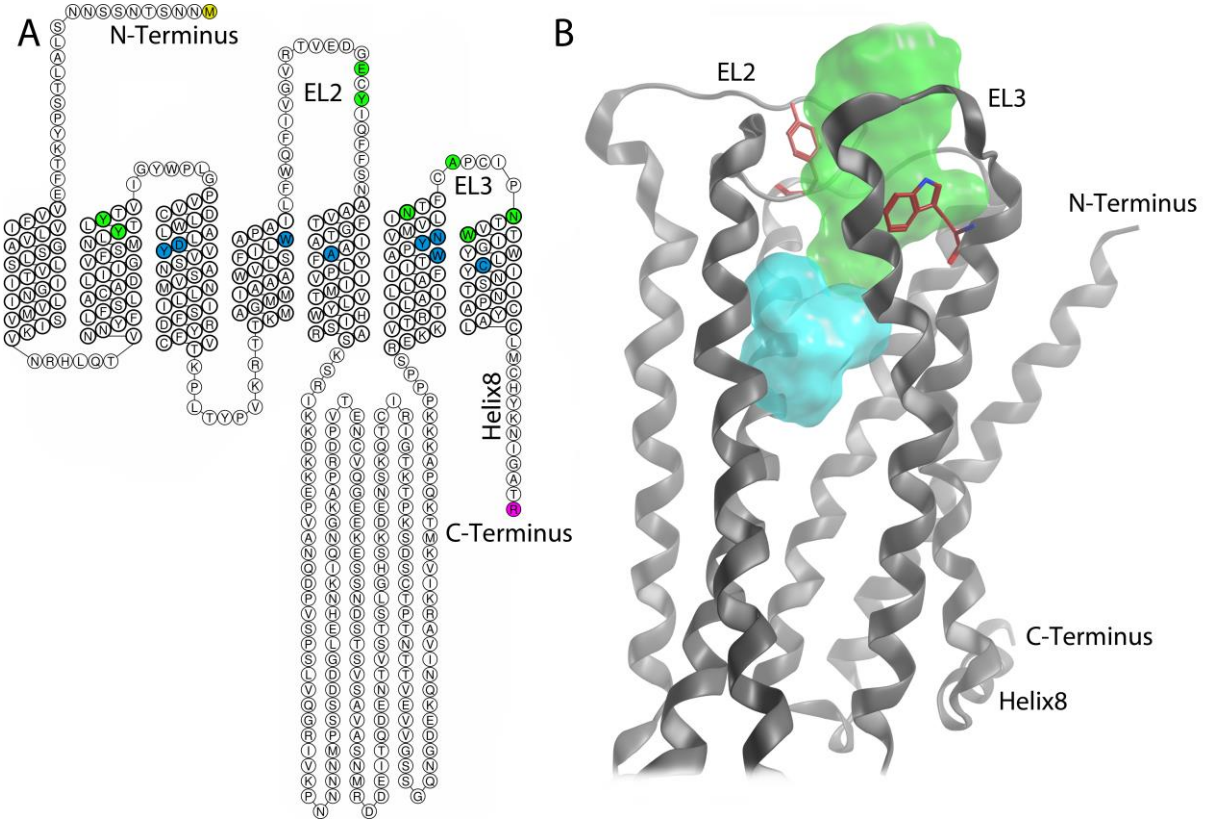


Figure 6: A: Snake plot of the $M_2$ AChR. Residues that contribute to allosteric ligand binding are shown in green. The most important residues for the binding of orthosteric ligands are shown in blue. The extracellular N-terminus is highlighted in yellow, the intracellular C-terminus is shown in magenta. This picture was made by using the GPCRdb [23]. B: Crystal structure of the $M_2$ AChR. The orthosteric binding pocket (blue) is located at the transmembrane core region. The allosteric binding site (green) lays in the extracellular region and is characterized by the allosteric key residues Y177 and W422 (red).

## 1.3 Crystallization of GPCRs

Due to the stabilizing effect of the membrane on the protein structure, the crystallization of GPCRs represents an obstacle for structural biology. Numerous efforts have been made to develop novel approaches for GPCR crystallography. Since the first resolved GPCR crystal structure in 2000, 135 crystal structures have been solved up to present (Figure 7). The first 14 crystal structures were non-human rhodopsin receptors. Since the first human GPCR structure was resolved in 2007, up to date 77 crystal structures are available for human GPCRs. Despite remarkable achievements in the last years, the crystallization of GPCRs remains a challenge [11]: GPCRs must be embedded in a membrane-like environment to retain structural integrity and their constitutive activity

results in high conformational flexibility [11]. Due to the exceptional absence of a basal activity for rhodopsin [24] this receptor is the first resolved crystal structure of a GPCR [25] and represents a breakthrough by providing a three-dimensional view on GPCRs for the first time. Subsequently, impressive progress in crystallography and protein engineering made it possible to determine more and more receptor structures [26]. Approaches for the crystallization of GPCRs include the insertion of thermostabilizing mutations, the insertion of the T4-lysozyme for stabilizing IL3, the stabilization with anti- or nanobodies and finally ligands that occupy the binding site with high affinity or irreversible binding [27]. The application and combination of these techniques led to the determination of more and more GPCR crystal structures, including the successful crystallization and structure elucidation of active-like receptor conformations (Figure 8).

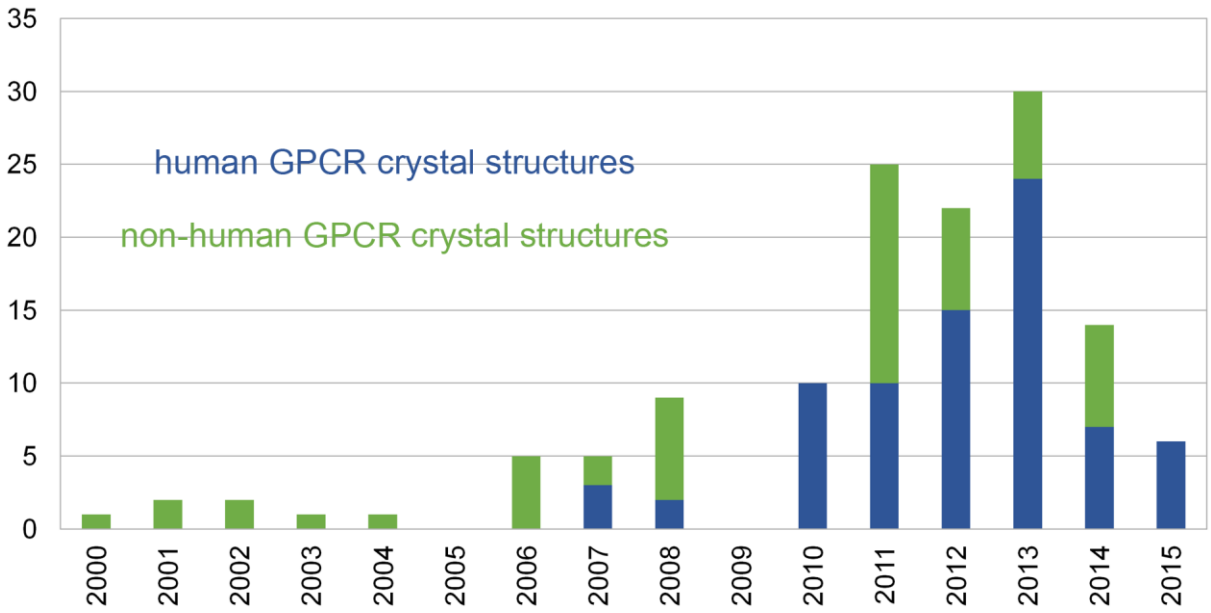


Figure 7: Novel crystallization techniques led to a remarkable increase of determined crystal structures in the last years (Data for 2015 include the period January to March).

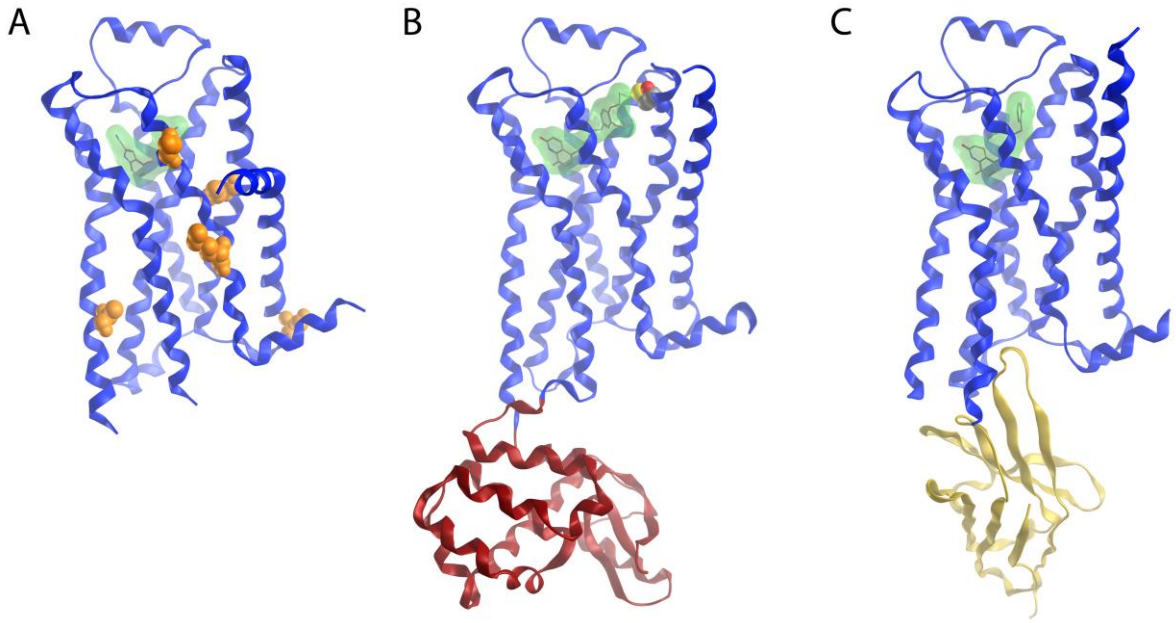


Figure 8: Approaches for GPCR crystallization include A: thermostabilizing mutations (orange) [28], B: irreversibly bound ligands and the insertion of $T_4$ lysozyme (red) [29] and C: the stabilization with nanobodies (yellow) [30].

The first successful crystallization of active-like receptors was achieved for the crystal structure of opsin in its G protein interacting conformation [31] and the $\beta_2$ adrenoceptor irreversibly bound to an agonist [29]. These structures allow insights in the general activation mechanism of GPCRs. Recently, the $M_2$AChR was resolved with an orthosteric agonist and an allosteric modulator simultaneously bound to the receptor [32]. The comparison of different resolved activation states shed light on structural properties and provides a deeper understanding of the activation process. Nevertheless, it is noteworthy that crystal structures always represent single static conformations of highly dynamic receptors and offer only limited insights regarding the whole conformational space and the resulting functionality [1].

## 1.4 GPCR signaling

GPCRs trigger multiple signal-switching mechanisms (Figure 9), which include G-protein activation, the binding of ß-arrestin proteins and other GPCR-interacting proteins (GIPs), like kinases. Therefore GPCRs can be described as integrative and highly dynamic signaling machines [16].

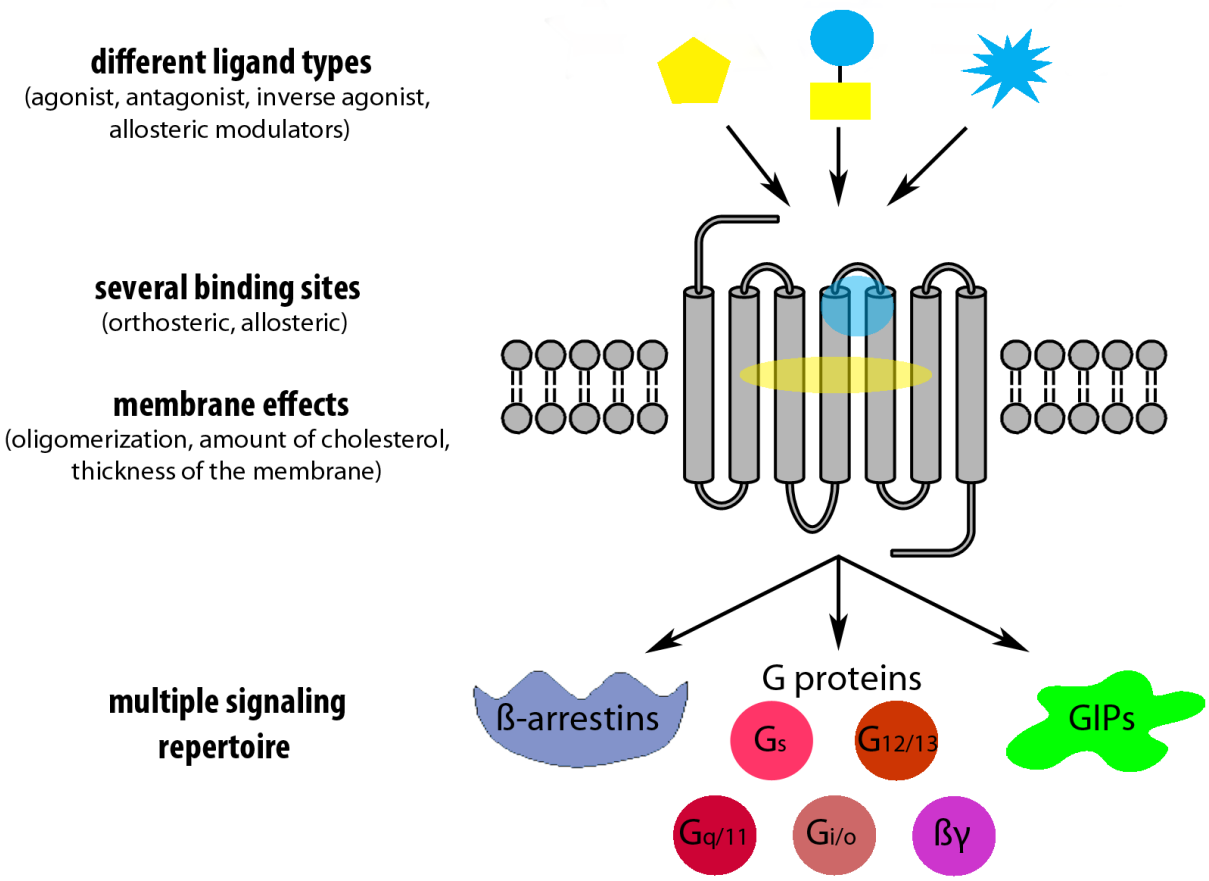


Figure 9: GPCRs are highly dynamic signaling machines: numerous distinct receptor conformations can be stabilized differently by a multitude of ligand types, which results in a highly complex signaling network.

The activation of a GPCR is characterized by conformational changes that expose intracellular epitopes for the interaction with signaling proteins. Besides basal activity, these changes of the receptor conformation can be controlled by ligands that can stabilize a distinct receptor conformation. An essential requirement for the various signaling pathways is flexibility of the receptor that allows the possible binding of different proteins on its intracellular side [33].

Regarding G-protein coupling, the activation of the receptor leads to an exchange of GTP for GDP bound to the Gα unit within the cell, followed by the dissociation of the Gα-GTP unit from Gβγ and coupling to effector enzymes [34]. Thus, the production of secondary messengers, like for example, cAMP, cGMP, DAG, and calcium ions can be induced or inhibited [35].

Most receptors prefer a distinct signaling pathway upon activation. MAChRs (Table 1), for example, can be divided in subtypes that prefer $G_i$-coupling ($M_2$ and $M_4$) or $G_q$-coupling ($M_1$, $M_3$ and $M_5$) [36]. Activation of the $M_1$, $M_3$, and $M_5$ receptor subtypes primarily results in coupling to the $G_{q/11}$ family of G proteins, which leads to an activation of phospholipase C (PLC), release of inositol-1,4,5-trisphosphate ($IP_3$), and subsequent mobilization of intracellular calcium [37]. The activation of the even-numbered receptor subtypes ($M_2$ and $M_4$) primarily results in the coupling of G proteins of the $G_{i/o}$ family, which leads to inhibition of adenylate cyclase (AC) and finally the reduction of cAMP-levels in the cell [33].

This naturally imprinted signaling preference can be shifted by specific ligands. Such biased ligands (also referred to as *functional selective ligands*) are able to stabilize a certain receptor conformation or a bundle of conformations linked to a specific signaling repertoire [38]. Remarkably, GPCRs respond to a broad spectrum of chemical entities, ranging from photons, ions, amines, lipids and nucleotides to peptides and proteins [39]. This high diversity of ligands has two consequences for drug design: (i) novel chemical entities that bind to GPCRs cover a huge chemical space, but (ii) they may allow for the binding to many different GPCRs rendering the design of specific ligands a challenge.

## 1.5 Therapeutic relevance of GPCRs

Signal transmission into cells is an essential part for the regulation of biological systems. Besides other protein classes, like ion channels or transporters, GPCRs represent a universal way to provoke a distinct intracellular reaction upon extracellular stimulation. GPCRs are expressed in nearly all kinds of tissues and contribute to the regulation of an enormous variety of physiological and pathophysiological functions [1]. This is also reflected by the huge amount of clinically used drugs that are addressing GPCRs: About 30% of all marketed drugs are directly acting on GPCRs [40]. These drugs are well established for the therapy of numerous diseases including central nervous system disorders, cardiovascular diseases, inflammatory diseases, cancer, metabolic imbalances and monogenic diseases among others [27, 41]. Furthermore, a lot of drugs that do not directly bind to GPCRs finally display their therapeutic effect through a GPCR. One example is the reduction of the availability of a physiological GPCR ligand through inhibition of an enzyme (e.g. angiotensin-converting-enzyme or acetylcholine-esterase (AChE)) involved in its endogenous synthesis [42, 43] or the modulation of neurotransmitter concentration (e.g. serotonin- or noradrenaline-transporters) [44]. Despite their high clinical impact, only a small fraction of human GPCRs have been successfully therapeutically targeted [7].

### 1.5.1 Therapeutic fields for MAChR ligands

MAChRs belong to the pharmacologically highly important *Rhodopsin* family. They consist of five subtypes ($M_1$-$M_5$ AChR) that are involved in a broad range of pathological conditions, such as chronic obstructive pulmonary disease, cognitive disorders, urinary incontinence and diabetes [45].

$M_1$ AChR is abundant in the brain and ganglia, $M_2$ AChR in the heart, $M_3$ AChR in glands, smooth muscle and the vascular endothelium, $M_4$ AChR in lungs and striatum, and $M_5$ AChR can be found in certain regions of the cortex and hippocampus [46, 47]. The differences in tissue distribution and intracellular signaling (Table 1) results in a variety of pharmacological effects, rendering MAChRs interesting therapeutic targets.

Table 1: Odd-numbered MAChR subtypes primarily couple with $G_q$-proteins, whereas the even-numbered prefer $G_i$-coupling upon activation, which results in a different second messenger pattern [46, 47]. The tissues with the highest expression levels are underlined.

| | **$M_1$ AChR** | **$M_2$ AChR** | **$M_3$ AChR** | **$M_4$ AChR** | **$M_5$ AChR** |
|---|---|---|---|---|---|
| **Preferred G-protein** | q/11 | i/o | q/11 | i/o | q/11 |
| **Second messenger** | PLC $IP_3$/DAG $Ca^{2+}$/PKC | AC (-) | PLC $IP_3$/DAG $Ca^{2+}$/PKC | AC (-) | PLC $IP_3$/DAG $Ca^{2+}$/PKC |
| **Locations** | Brain<br>Ganglia | <u>Heart</u><br>Hindbrain<br>Smooth muscle | <u>Smooth muscle</u><br>Glands<br>Brain | Basal forebrain<br>Striatum<br>Lungs | <u>Brain</u><br>Substantia nigra |

Unfortunately, all available MAChR-interacting drugs lack pronounced subtype selectivity, because of the high conservation of the orthosteric binding pocket [48] (see also chapter 4.1.1 and Figure 6B). Additionally, MAChRs represent important off-targets that are connected to adverse side effects for a broad range of clinically used drugs, including dry mouth, blurred vision, tachycardia, decreased intestinal motility and constipation [47, 49].

Historically, Atropine (**3**) played an important role as anticholinergic drug. It is known for its long tradition as one of the classic poisons of antiquity, and the effect of pupil dilatation (mydriasis), which was the reason to name the plant *Atropa belladonna* [50]. This explains the usage of anticholinergic drugs in ophthalmology, whereas today Tropicamide replaced Atropine (**3**) as mydriatic drug. Beyond mydriasis the MAChRs are also important as ophthalmic drug targets in the therapy of glaucoma and myopia [51]. Beyond the applications as ophthalmic drugs, various (patho)physiological functions can be modulated by targeting MAChRs. The following section gives an overview on therapeutic fields for MAChR ligands ordered by organ systems.

*Pulmonary system:* In the lungs, anticholinergic compounds block muscarinic receptors ($M_2$/$M_3$ AChR) on the airway smooth muscle, glands and nerves to influence muscle contraction, gland secretion, airway inflammation and airway remodeling [52]. Muscarinic antagonists (e.g. Tiotropium (**2**)) are therapeutically used as bronchodilators to treat lung diseases characterized by airflow obstruction and underlying airway inflammation like COPD and asthma [53]. The bronchoconstriction of ACh is predominantly mediated by $M_3$ AChR, but interestingly $M_2$ AChR was shown to serve as inhibitory autoreceptor for the limitation of ACh release [54].

*Cardiovascular system*: The parasympathetic stimulation of $M_2$ AChR results in a decreased cardiac output by decreasing the heart rate [55]. Therefore muscarinic antagonists and inverse agonists can increase the heartrate as a result of an anticholinergic side effect or as a desired clinical effect.

*Urinary bladder*: ACh in the bladder is not only released from postganglionic parasympathetic nerves, but also from the urothelium in an auto- and paracrine manner, which indicates the important role of muscarinic receptors for the urinary bladder function [56]. Muscarinic antagonists and inverse agonists ($M_3$ AChR) like tolterodin or darifenacin are used for the treatment of overactive bladder symptoms [57].

*CNS*: Despite the fact that MAChRs are widely expressed in the central nervous system controlling a variety of neuronal functions, the only MAChR ligands approved for clinical use are non-selective antagonists for the treatment of Parkinson's disease [58]. The various CNS functions of MAChRs encourage their evaluation as possible drug targets. Due to the complexity of brain functions influenced by MAChRs and the low subtype selectivity of known drugs, it becomes obvious that more specific ligands are needed to further evaluate the role of ACh in CNS disorders. The activation of the central muscarinic receptors $M_2$/$M_4$ leads to antinociception, making selective $M_2$/$M_4$ agonists suitable analgesic drug candidates [59]. The stimulation of $M_1$/$M_4$ receptors may provide therapeutic benefit in schizophrenia and drug addiction [58, 60].

The clinical use of AChE-inhibitors like donepezil, galantamin and rivastigmine for the treatment of Alzheimer's disease [61] suggests a potential therapeutic benefit for ligands that modulate MAChRs. The most promising ways for new AD drugs are $M_1$ AChR agonists and $M_2$ AChR antagonists (inhibitory autoreceptor) [58].

*Cancer:* Studies with knockout mice support the concept that subtype-selective MAChR antagonists ($M_1$/$M_3$ AChR) may prove to be clinically useful for the treatment of certain forms of cancer, like colon neoplasia or prostate cancer [62].

*Pancreas*: MAChRs were shown to influence the pancreatic β-cell function and suggest that the $M_3$ AChR mediated activation of arrestin-dependent β-cell pathways may further enhance insulin secretion [62].

*GIT*: Hyoscine butylbromide is the only OTC drug (in many countries) that acts on MAChR and is well known for its spasmolytic effects on smooth muscle cells in abdominal cramping and pain [63].

Taken together, MAChR are highly interesting and important targets for various clinical applications. Unfortunately, their therapeutic potential cannot be utilized yet, because available ligands lack subtype selectivity.

# 2 Aim and objectives

G-protein coupled receptors are hepta-helical proteins transferring information across a membrane, which allows cells to communicate. They trigger multiple signal-switching mechanisms like G-protein activation, binding of ß-arrestin proteins and activation of kinases. The understanding of conformational changes resulting in these activations is still incomplete and represents a major challenge for the design of specific GPCR modulators.

This research project aims at the elucidation of structural characteristics that are responsible for receptor function. A special focus was set on the mechanisms that are able to modulate receptor response in a ligand-dependent manner. For this purpose, muscarinic acetylcholine receptors were chosen as model system to answer the following questions:

1. How are MAChRs able to bind a broad range of chemical entities, which makes them an off-target for clinical drugs and pharmacological tools?
2. What structural elements distinguish between the five MAChR subtypes?
3. What are the structural requirements for subtype selective ligands?
4. Is it possible to activate the receptor up to a certain degree? What binding mode differences trigger this partial agonism?
5. How are ligands able to stabilize a conformation that is linked to a distinct signaling pathway?

The clarification of these questions should lead to a deeper understanding of the structural and functional properties of MAChRs that are the basis of a ligand-dependent modulation.

In order to address these questions, structural and functional models of MAChRs in complex with different ligands should be built and investigated by using state-of-the-art molecular modeling techniques.

# 3 Computational methods

By now, computational tools have become invaluable for drug design campaigns but also as auxiliary tool for structural biology [1]. The broad diversity of computational methods that are successfully applied for drug design suggests that no fundamentally superior techniques exist. The target protein, available data, and available resources highly influence the performance of available methods [64]. Due to their illustrative power, structure-based approaches (relying on experimentally determined structures or on structural models) are commonly preferred over purely ligand-based approaches. However, in terms of predictability, structure-based approaches are not necessarily considered superior [65]. This chapter will give an overview on the computational methods that were applied in this study: Homology modeling (HM), docking, 3D-pharmacophore analysis and molecular dynamics (MD) simulations (Figure 10).

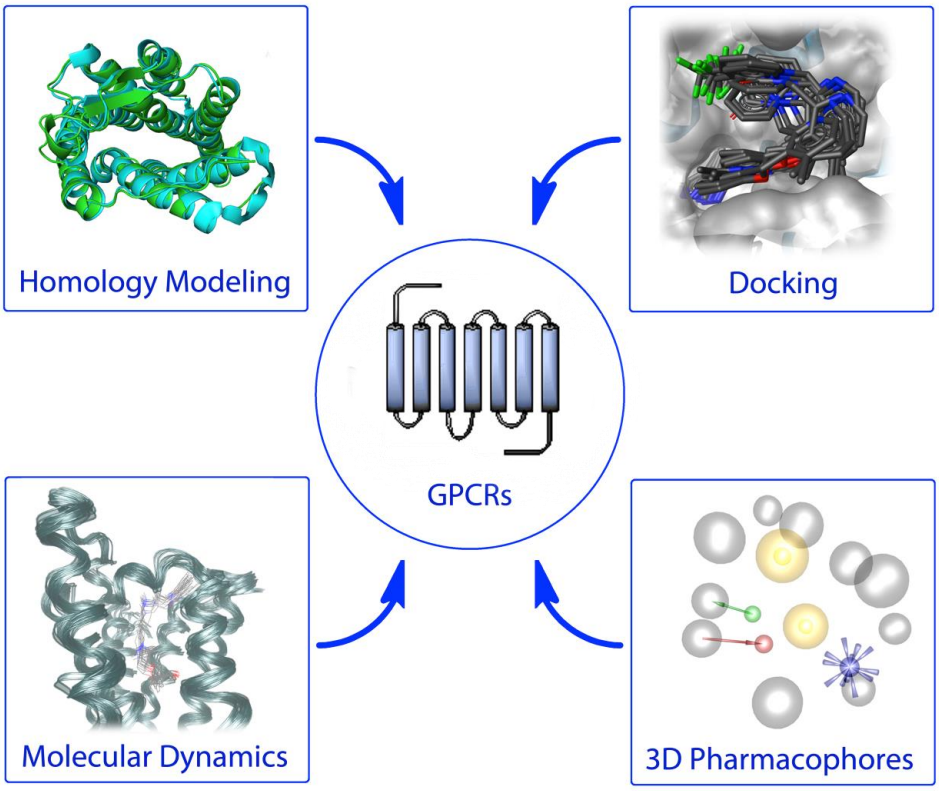


Figure 10: Overview of computational tools used in this study.

## 3.1 Homology modeling

Homology modeling (HM) is a widely used approach to obtain structural models in the absence of a crystal structure, which aligns the sequence of the protein with an unknown 3D structure onto a template with an experimentally determined structure [1]. GPCRs represent a promising protein class for HM, because of the similar overall architecture of the transmembrane domains, although sequence similarities are quite low [66]. Due to this low sequence similarity, HM have to be refined and evaluated very carefully before using them for structure-based approaches in drug design campaigns. The search for the right template structure considers similar evolutionary origin and a preferably high sequence similarity. The sequence alignment of the template structure and the target protein is the most critical part [67]. An essential step is the identification of the most conserved residue of each helix and other highly conserved motifs as anchor points for the right protein architecture [66] (Figure 11). This illustrates why the right alignment is crucial for the construction of missing atom coordinates for the homology model.

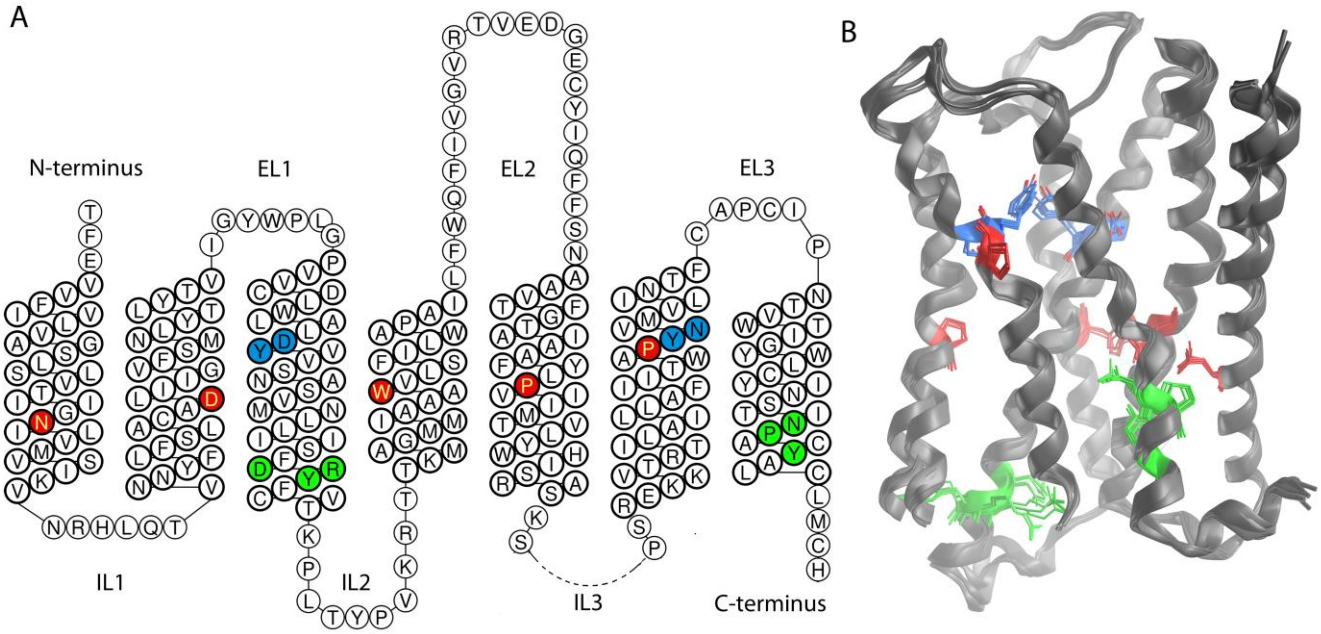


Figure 11: Highly conserved residues serve as anchor points for HM. A: snake plot of the $M_2$ AChR, B: Superimposition of 3D structures of all MAChR subtypes in their inactive state. A and B: The highly conserved motifs DRY and NPxxY are shown in green, the key residues for orthosteric binding are shown in blue and the most conserved residues of other TM are shown in red color.

Three main approaches are pursued to obtain the structural model, (i) by assembly of rigid bodies, (ii) by segment matching or coordinate reconstruction and (iii) by satisfaction of spatial restraints [67]. The initially obtained homology models should be carefully refined and validated. This can include protein geometry tools, re-docking of known ligands, molecular dynamics simulations, and virtual screening experiments. Additionally, mutational data, if available, can help to identify key residues and elucidate their role for ligand binding which also helps to evaluate the homology model. All homology models presented in this study were obtained by using the homology modeling tool from MOE (*Molecular Operating Environment (MOE)*, 2014.09; Chemical Computing Group Inc.)

## 3.2 Molecular docking

Molecular docking is frequently used as a standard tool in structure-based drug design to predict binding conformations of small molecules within a known binding site of a protein target [68]. The basic steps of a docking algorithm include a geometric search and a scoring function [69]. The search algorithms share the strategy to geometrically fit a ligand into the binding site that is mostly assumed to be rigid [70]. Therefore, different strategies have been implemented, including stochastic methods, genetic algorithms, Monte Carlo optimization, ligand fragmentation, molecular shape or three-dimensional molecular similarity [71]. In order to assess the quality of the obtained poses, empirical, force-field-based, knowledge-based and consensus scoring functions can be applied [64]. Whereas pose generation works reliably to sample possible ligand geometries, the performance of scoring functions heavily varies depending on the target protein, mainly due to the challenging task of predicting the entropic component of ligand binding [69]. The main application areas for docking in drug design are virtual screening and binding mode investigations. Widely used docking programs include AutoDock [72], DOCK [73], FlexX [74], Glide [75], GOLD [76], and ParaDockS [77]. All docking experiments in this study were performed with the CCDCs software GOLD 5.1 [76]. In this docking software ligand placement and pose optimization is based on a genetic algorithm. The employed scoring function GoldScore [76] is a molecular mechanics-like function with terms for protein-ligand hydrogen bonds, intramolecular hydrogen bonds, protein-ligand van der Waals energy and intramolecular van der Waals energy. The final fitness score is a weighted sum of all the energy components [78]. The weights are determined by empirical adjustment to best reproduce known protein-ligand complexes [79].

## 3.3 Molecular dynamics

Molecular dynamics simulations have become a major technique for the development of novel bioactive molecules and for the investigation of their mode of action [80]. MD is an *in silico* method that utilizes structural data to sample possible conformations of macromolecular systems and the different paths between each of them [1]. These simulations represent a protein-ligand complex by molecular mechanics using a description of atoms and bonds that relies on Newtonian mechanics [64]. In classical MD simulations, the potential energy function commonly denoted as the 'force-field' describes the interactions between the particles (atoms) [80]. The used force fields are typically designed based on a combination of first-principles physics and parameters fitting to quantum mechanical computations and experimental data [81]. The time series can also be viewed as a statistical-mechanical ensemble of configurations, which allows studying dynamic processes. By averaging over this ensemble, thermodynamic properties of a system can be estimated [80]. Therefore MD simulations provide an invaluable source of structural and functional information. The most established MD software suites include GROMACS [82], CHARMM [83], AMBER [84], NAMD [85] and Desmond [86]. The high value of MD is reflected by the broad application scenarios ranging from studies that are focusing on ligand binding (entry-exit, specificity, binding mode) to investigations of conformational flexibility and mechanistic models [80]. All MD simulations presented in this study were carried out with Desmond 3.1 [86].

## 3.4 3D pharmacophore analyses

The term pharmacophore was defined by the IUPAC as an ensemble of steric and electronic features that is necessary to ensure the optimal supramolecular interactions with a specific biological target structure and to trigger (or to block) its biological response [87]. In principle, a 3D pharmacophore model is a spatial arrangement of chemical features, such as hydrogen bonds, aromatic rings, charges and hydrophobic contacts, representing the essential interactions of small organic ligands with a macromolecular receptor [88]. The core idea of “stripping” functional groups off their actual chemical nature in order to classify them into very few pharmacophore types is both the main advantage and the main drawback of pharmacophore modeling [89]. 3D pharmacophores are easily understandable and simple to modify, which allows researchers to incorporate their knowledge about a specific binding mode into a transparent, but still highly descriptive model [71]. Therefore 3D pharmacophores can be used for the retrospective explanation of ligand binding modes and ligand affinities but also as a powerful tool for prospective virtual screening. Several pharmacophore modeling programs are available, such as LigandScout [88, 90], Catalyst [91], Phase [92] or MOE [93]. In this study, LigandScout 3.1 was applied for all pharmacophore modeling experiments. The software LigandScout [88, 90] obtains pharmacophores from protein-ligand complexes, interprets ligand geometries, assigns correct hybridization states and applies a set of rules that classifies plausible protein-ligand interactions [71] and is therefore a strong tool for binding mode investigations but also for the evaluation of docking poses.

# 4 Results

## 4.1 Structural models of all MAChR subtypes

The crystal structures of the inactive $M_2$AChR [94] and $M_3$AChR [95], but also active receptor states for $M_2$AChR [32] have been determined recently. These crystal structures represent the best available templates for homology modeling of the closely related subtypes because of their high sequence similarity (Figure 12). In this study, the active receptor conformation of $M_2$AChR [32] was used as template structure for the generation of active-like models for the other subtypes. The inactive receptor structure for $M_4$ AChR was modeled on the basis of the inactive $M_2$AChR [94], whereas the crystal structure of $M_3$AChR [95] served as template for HM of the inactive $M_1$ AChR and $M_5$ AChR. The initial structural models were derived by the homology modeling tool of MOE (*Molecular Operating Environment (MOE).*

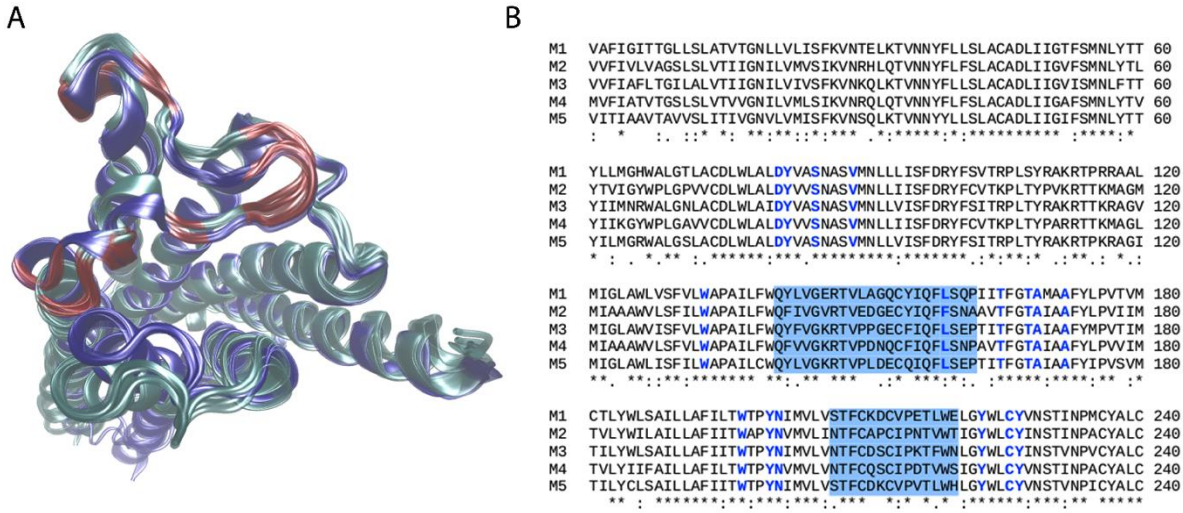


Figure 12: A: Superimposition of the five MAChR subtypes. Inactive structures are shown in cyan, active structures in blue, non-conserved epitopes of EL2 are shown in red. B: Sequence alignment of the $M_1$-$M_5$ AChRs; residues of the EL2 and EL3 are highlighted in blue, the residues of the orthosteric binding site are shown in blue letters; stars indicate for identical, dots and colons for similar residues.

In order to assess model quality, the initially derived models were analyzed in terms of protein geometry with a special focus on typical dihedral angels shown in Ramachandran plots [96]. In a next step, short MD simulations of the HMs were carried out to refine model structures and assess their conformational stability. The Ramachandran plot of the initial models indicated some atypical geometries (Figure 13A) that could be resolved during the MD-based refinement (Figure 13B). Subsequently, the refined models were used for re-docking experiments with known ligands (QNB (**1**), Iperoxo (**5**)). The obtained docking poses were similar compared to the co-crystalized ligands (Figure 13C) and showed a similar orientation and interaction pattern.

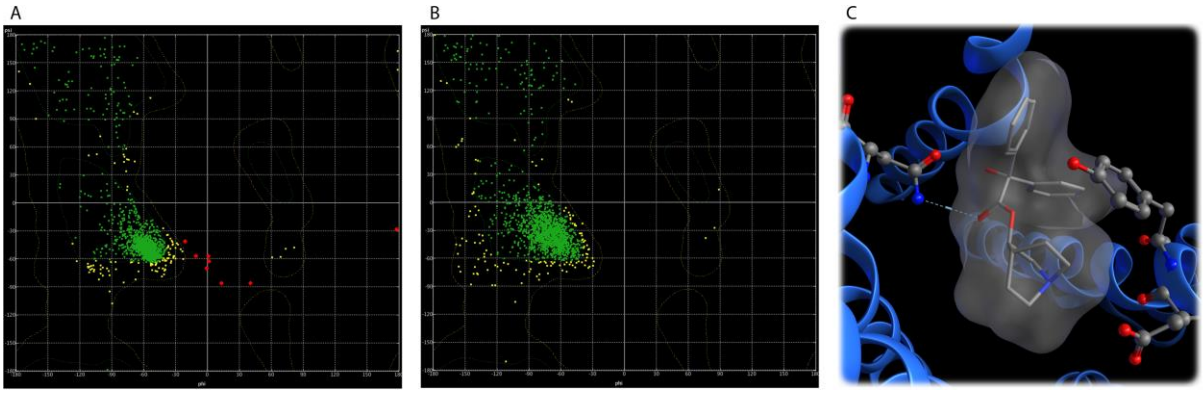


Figure 13: The Ramachandran plot for the initially derived HM indicate a few outliners (shown in red, A). After MD-based model refinement, no outliners could be observed in the Ramachandran plot (B). Re-docking of known ligands (QNB (**1**)) showed comparable binding modes like the co-crystallized ligand.

*MD based structure refinement:* The initial homology models were used as starting points for a MD-based structural refinement including the sampling of protein flexibility [36]. These MD simulations indicate the transmembrane domains and the orthosteric binding pocket to be mostly rigid whereas the extracellular loops (EL2 and EL3) show much more flexibility (Figure 14). This result was expected due to the stabilizing effect of the membrane. However, our simulations structurally illustrate the conformational variability of EL2 and EL3 that contain allosteric epitopes, which represent an interesting starting point for subtype-specific binding mode investigations.

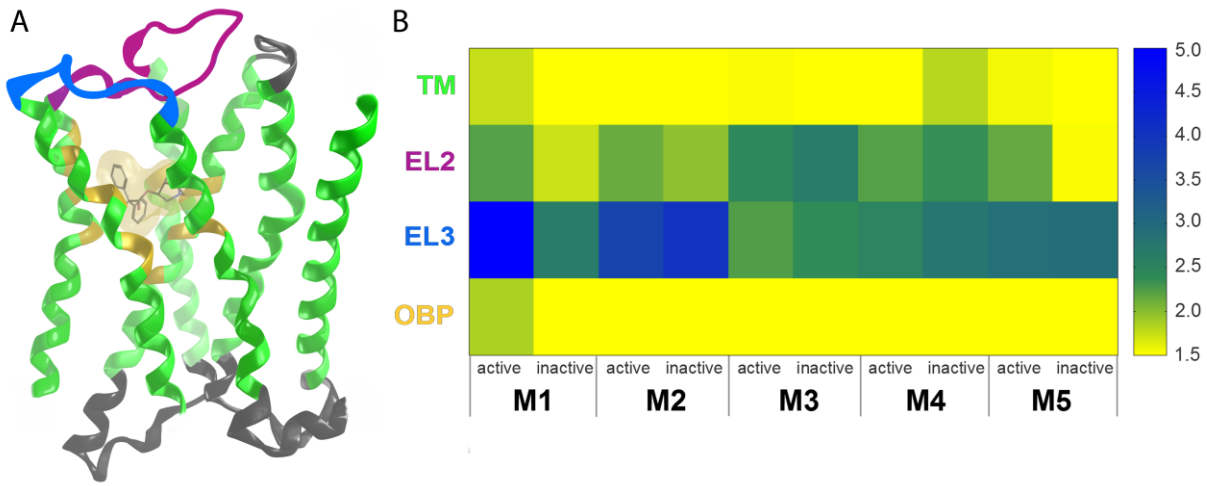


Figure 14: A: Crystal structure of the $M_2$ AChR with the transmembrane (TM) regions (green and yellow), EL2 (red), EL3 (blue) and the residues of the orthosteric binding pocket (yellow). B: Heat map of geometric deviations (max. RMSD values [Å]) for TM, the orthosteric binding pocket (OBP) and the extracellular loops (EL2/EL3) calculated by MD simulations.

### 4.1.1 The promiscuous orthosteric binding site

A comparison of the available crystal structures [94, 95] but also homology models of MAChRs [36] show the high structural conservation of the orthosteric binding pocket and indicate key residues for ligand binding (Figure 15).

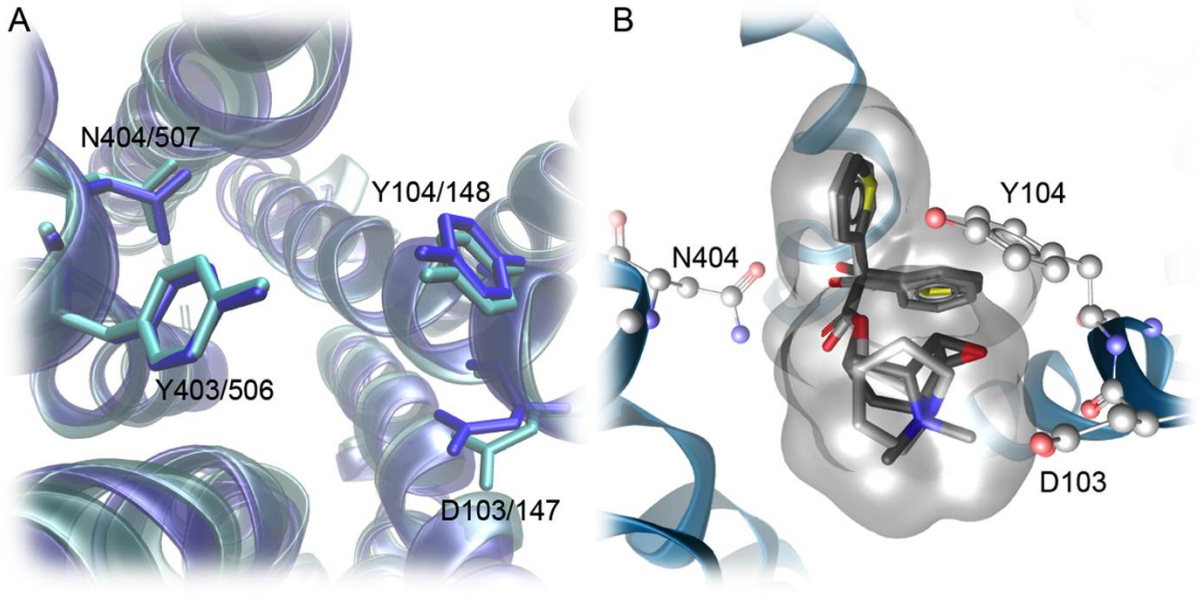


Figure 15: A: Comparison of the crystal structures of $M_2$AChR (dark blue) and $M_3$AChR (light blue) with key residues for ligand binding (the first number is for $M_2$AChR and the second for the corresponding residue in $M_3$AChR). B: Superimposition of QNB (**1**) (light gray) in the $M_2$AChR crystal structure and Tiotropium (**2**) (dark gray) in its co-crystallized conformation.

3D pharmacophore analysis illustrates the binding mode of (3R)-1-azabicyclo[2.2.2]oct-3-yl-hydroxy(diphenyl)acetate (QNB (**1**)), the co-crystallized ligand in the $M_2$ AChR structure (Figure 18A). The important aspartic acid D103 (and corresponding residues) is capable to form an electrostatic interaction with a positive ionazable motif that can be found in all known ligands like QNB (**1**) in $M_2$AChR, or Tiotropium (**2**) in the $M_3$AChR structure [95]. This interaction strongly affects the general orientation of a ligand in the binding pocket. The aromatic rings of QNB (**1**) and Tiotropium (**2**) fill two hydrophobic pockets that also belong to the orthosteric binding site. QNB (**1**) and Tiotropium (**2**) both show the same orientation and binding modes and therefore form a suitable reference for the interpretation of docking results (Figure 15B). The analysis of docked Atropine (**3**) and Scopolamine (**4**) by using 3D pharmacophores illustrates their orthosteric ligand binding mode and (Figure 16). D103, W400 and Y403 allow for electrostatic interactions with the nitrogen of the tropane ring system of Atropine (**3**) and Scopolamine (**4**). In Atropine (**3**) the carbonyl group of the ester moiety acts as hydrogen bond acceptor and the hydroxyl function as hydrogen bond donor for N404. In Scopolamine (**4**) the oxygen of the epoxide serves as hydrogen bond acceptor for C429, resulting in a different arrangement of the tropane ring system (see also chapter 4.2.1). Additionally, the hydroxyl function in Scopolamine (**4**) acts as hydrogen bond donor for A194. The phenyl ring of Atropine (**3**) is embedded in a lipophilic pocket formed by V111, W155, A194 and W400 whereas the phenyl ring of Scopolamine (4) shows hydrophobic contacts with Y104, F181, T187, A191, V407 and Y403. In order to confirm the proposed binding mode, MD simulations of the $M_2$AChR in complex with Atropine (**3**) and Scopolamine (**4**) were carried out. During the 20 ns of simulation the general ligand orientation did not change, which results in a low geometry deviation (Figure 16C). The protein-ligand interactions described above could also be found in the trajectory. The electrostatic key interaction with D103 could be observed during the whole simulation.

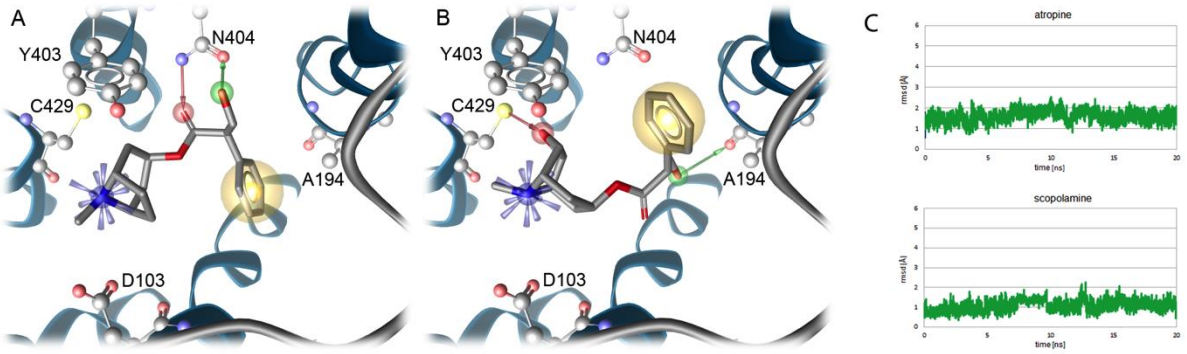


Figure 16: 3D pharmacophore analysis of Atropine (**3**) (A) and Scopolamine (**4**) (B) in the $M_2$AChR. Yellow spheres indicate lipophilic regions, red arrows hydrogen bond acceptors, green arrows hydrogen bond donors and positive ionazable centres are shown as blue stars. C: overall geometry deviation of backbone atoms of Atropine (**3**) and Scopolamine (**4**) during a 20 ns MD simulation.

The high conservation of the orthosteric binding site, which includes two lipophilic pockets allows for the potential binding of a diverse set of chemical entities. A broad range of marketed drugs show anticholinergic side effects (Figure 17).

Typical examples are Promethazine (**18**) (first-generation antihistamine, Figure 18B), Amitriptyline (**19**) (tricyclic antidepressant, Figure 18C) and Clozapine (**20**) (atypical antipsychotic, Figure 18D) [47, 49, 97]. Docking experiments with these CNS active drugs unveiled a matching interaction pattern comparable to QNB (**1**) (Figure 18). The general orientation in the binding site was similar and the key interaction of D103 with a positive ionazable center was found for all three drugs. Furthermore, both lipophilic pockets were addressed in a comparable manner by aromatic systems. This result shows the importance of MAChRs as off-targets for therapeutic drugs on a molecular level.

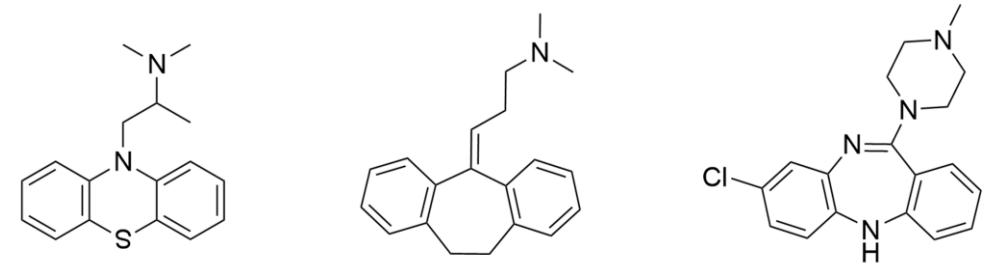


Figure 17: 2D representations of marketed drugs with anticholinergic side effects.

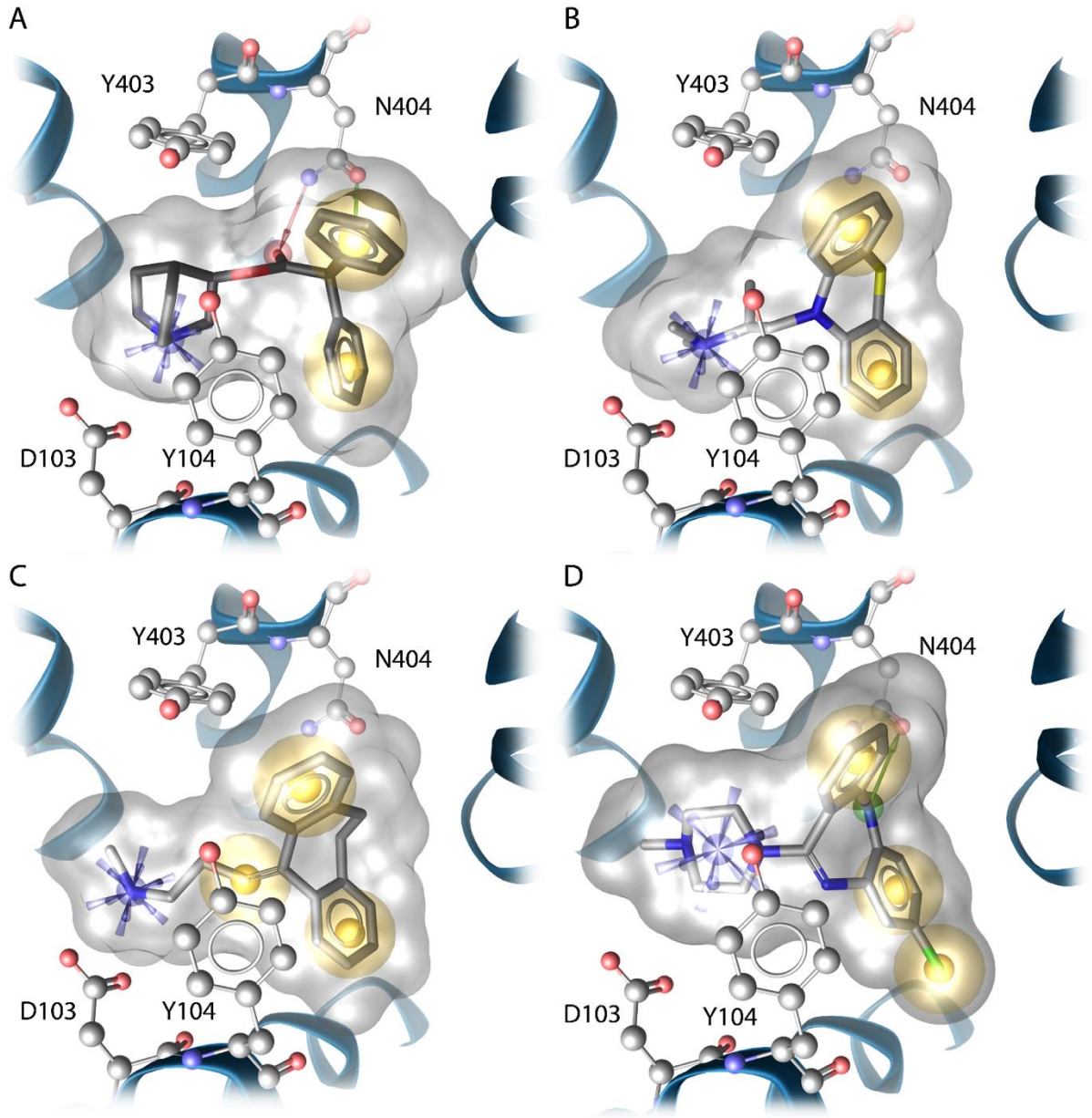


Figure 18: Co-crystallized ligand QNB (**1**) (A) and marketed drugs with anticholinergic side effects. Promethazine (**18**) (B), Amitriptyline (**19**) (C) and Clozapine (**20**) (D) share a common binding mode. Yellow spheres indicate lipophilic regions, red arrows hydrogen bond acceptors and positive ionizable centers are shown as blue spheres.

MAChRs have to be considered as off-targets not only for therapeutic drugs but also for pharmacological tools. NSC23766 (**6**), an inhibitor of Rac1 activation was found to show competitive antagonism at MAChRs similar to Methylene blue (**7**) [48]. Rac1 is involved in the control of many different cellular processes, including actin cytoskeleton reorganization, adhesion, migration, polarity, gene expression, and cell cycle progression[48]. NSC23766 (**6**) is used to chemically knock-out Rac1 to investigate

intracellular processes. The binding of NSC23766 (**6**) to MAChR may influence these processes in a Rac1 independent manner and has therefore be considered in these experiments. Docking experiments and 3D-pharmacophore analyses unveiled the binding mode of NSC23766 (**6**) to $M_2$ and $M_3$ AChRs. The general ligand orientation is highly similar in both receptors (Figure 19) although marginal differences could be observed [48], as described below.

The positive ionazable nitrogen of the tertiary amine allows for an electrostatic interaction with D103, Y104, Y403 and W400 in $M_2$ AChR and with D147, Y148, Y506 and Y529 in $M_3$ AChR. The nitrogen in position 3 of the pyrimidine ring serves as hydrogen bond acceptor for Y104 and Y403 for the $M_2$ AChR and for Y148 and Y506 in the $M_3$ AChR. The methyl group of the aliphatic chain is embedded in a hydrophobic pocket that differs between the subtypes: For $M_2$ AChR it consists of A191, F195, W400 and Y403, whereas Y148, W199 and W503 build that pocket for $M_3$ AChR. The quinoline ring lays opposite to T187 and W422 in $M_2$ AChR and opposite to Y506 and W525 in $M_3$ AChR. The methyl group of the pyrimidine ring shows hydrophobic contacts with the following residues: W155, F181, T187, T190 and A191 in $M_2$ AChR and with W199, T234, A235 and A238 in the $M_3$ AChR.

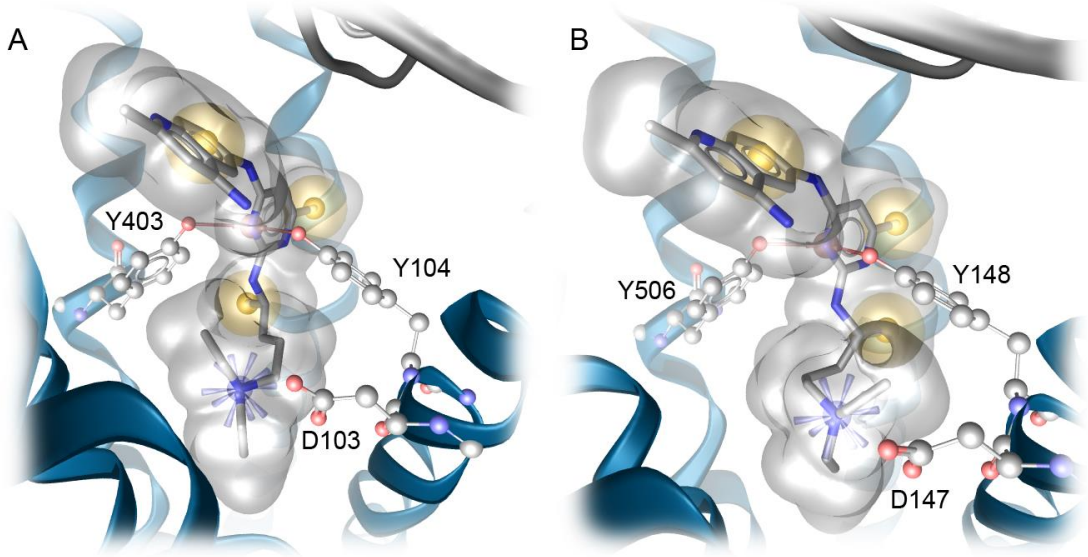


Figure 19: A: 2D structure of NSC23766 (**6**); B/C: 3D-pharmacophore analysis of NSC23766 (**6**) in the in the $M_2$AChR (B) and in the $M_3$AChR (C). Yellow spheres indicate lipophilic regions, red arrows hydrogen bond acceptors, green arrows hydrogen bond donators and positive ionazable centers are shown as blue spheres.

3D-pharmacophore analysis of Methylene blue (**7**) indicates the same binding mode for the $M_2$AChR and the $M_3$AChR (corresponding $M_3$ residue numbers are written in brackets) [48]. The positive ionazable nitrogen of Methylene blue (**7**) shows the key interaction with D103 (D147) and additionally with Y403 (Y506) and W400 (W503). The thiazin nitrogen serves as hydrogen bond acceptor for N404 (N507). V111 (V155), A194 (A238) and W400 (W503) lay opposite to one of the phenyl rings. W155 (W199), V111 (V155) and A194 (A238) build a pocket for the dimethylamino group (Figure 20).

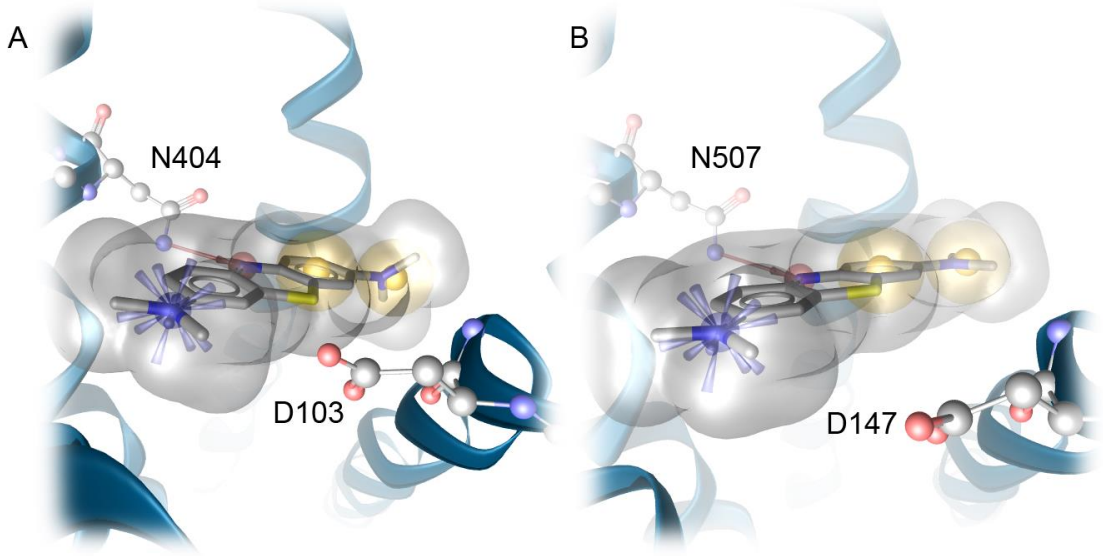


Figure 20: A: 2D structure of Methylene blue (**7**); B/C: 3D-pharmacophore analysis of Methylene blue (**7**) in the M2AChR (B) and in the $M_3$AChR (C). Yellow spheres indicate lipophilic regions, red arrows hydrogen bond acceptors and positive ionazable centers are shown as blue spheres.

### 4.1.2 Structural characterization of allosteric MAChR binding sites

The resolved crystal structures of the active and the inactive receptor state [32, 94] and available mutations (Y104A, Y177A, Y177Q, W422A) make the $M_2$ receptor a model example for GPCRs in several studies [98, 99]. The key residues for allosteric binding are Y177 and W422, which lay opposite to each other in the extracellular vestibule (Figure 6). Therefore the Cα-distance between these two residues (and their corresponding residues in other subtypes) can serve as an indicator for the characteristics of the allosteric binding site. The inactive receptor states show a higher Cα distance of these residues than active-like conformations, which is in accordance with available crystal structures and the general model of receptor activation [36]. Surprisingly, the distance changes between active-like and inactive structures are higher in $M_2$ and $M_4$ AChR than in $M_1$, $M_3$ and $M_5$ AChR. This observation corresponds to the experimentally observed preferred coupling mechanism ($G_i$ vs. $G_q$) but also with higher sequence similarities between the subtypes (Figure 21).

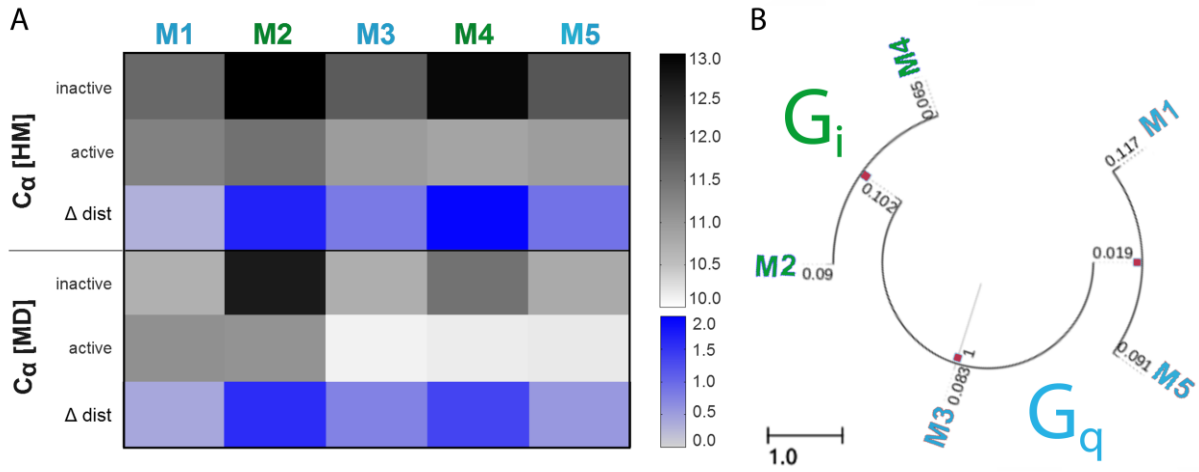


Figure 21: A: Heatmap of Cα distances (Å) of the allosteric key epitopes $M_2$Y177 and $M_2$W422 and their corresponding residues for the initial homology models (Cα [HM], above) as well as minimum distances observed in MD simulations (Cα [MD], below). B: Phylogenetic analysis of MAChR subtypes.

Potential epitopes that contribute to subtype selectivity can easily be located by sequence alignment, but these methods are not able to give a deeper understanding of functionality. In contrast, our obtained homology models are able to show structural characteristics of the five MAChR subtypes [36]. The highly conserved transmembrane domains and the orthosteric binding pocket turned out to be highly similar for all subtypes. However, the $M_2$ AChR shows a special feature: F181 that contributes to orthosteric ligand binding represents a unique residue at the end of EL2. All other subtypes contain a leucine at this position (Figure 22A). A structural comparison of the orthosteric binding pocket with the closely related $M_4$ AChR unveils similar side chain orientations, except $M_2$ D103/$M_4$ D84. However, space requirements and chemical functionality for phenylalanine and leucine are comparable and the side chain position of the aspartic acid is flexible. Therefore, these epitopes lose their ability to contribute to subtype selectivity.

A closer look at EL2 reveals a cluster of three neighboring acidic residues for the $M_2$ receptor (Figure 22B). This characteristic EDGE motif was previously shown to be involved in allosteric binding by mutational studies [100]. This part of the EL2 represents one of the most variable receptor segments among the 5 MAChR subtypes. Acidic residues are absent in this part for $M_1$, whereas one can be found in $M_3$ and $M_4$ AChR and two in the $M_5$ AChR. The glutamic acid in position 219 of the M3 receptor plays a special role, because it is able to form a salt bridge with a lysine at the N-terminal end of EL3 (Figure 22D). This results in a connection of EL2 and EL3 that has been found in both, the inactive crystal structure [95] and the active-like model. This result illustrates the steric constraints that allosteric binding moieties are subjected to. Additionally, allosteric binders are supposed to connect EL2 and EL3 through interactions with both, similar to the found salt bridge.

The above-mentioned key epitope Y177 in the $M_2$ receptor is potentially able to form π-π and π-cation-interactions with allosteric moieties. The corresponding residues of $M_1$(Y), $M_3$(F) and $M_4$(F) have the same ability, but the $M_5$ receptor containing a glutamine at this position loses this functionality, although it can serve as hydrogen bond donor or acceptor (Figure 22C).

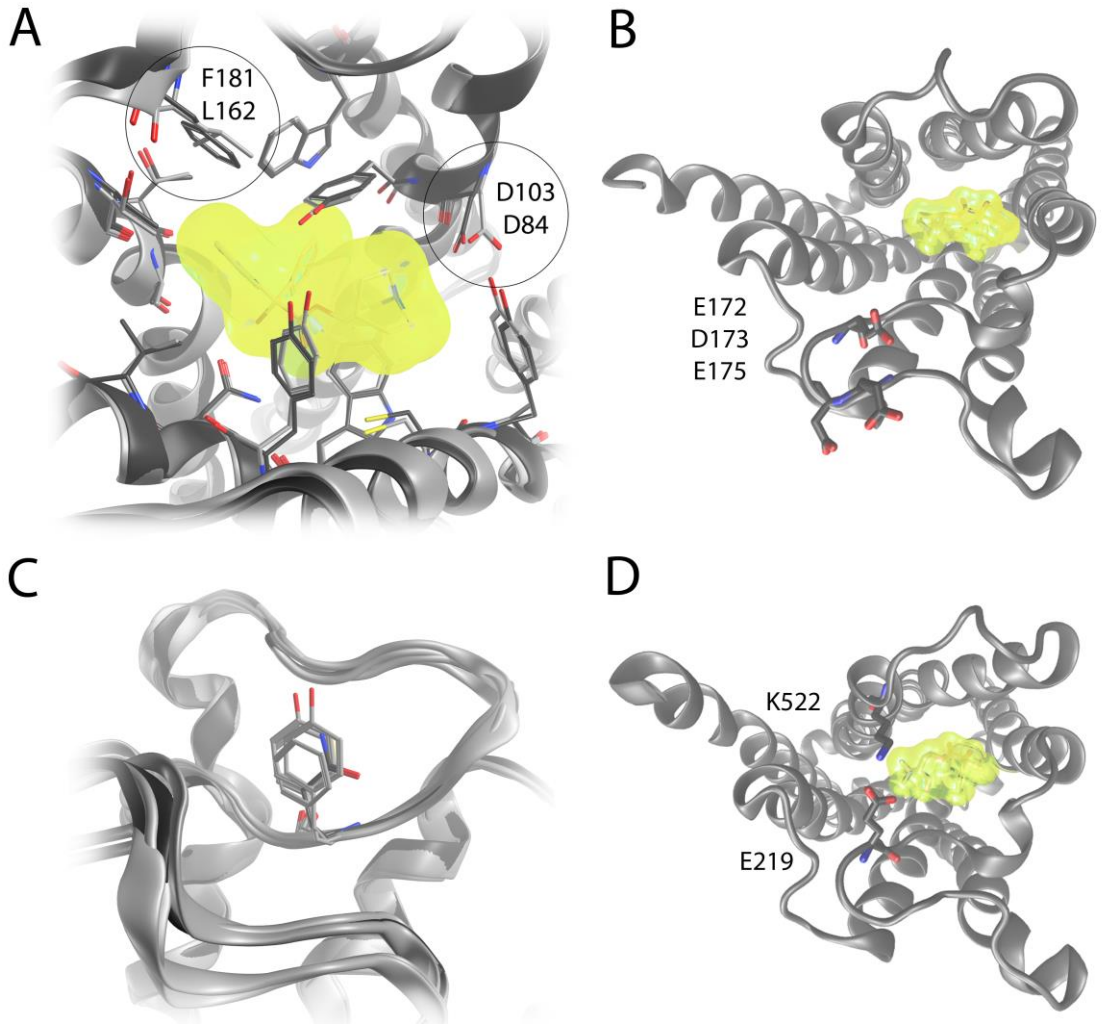


Figure 22: A: Structural comparison of the orthosteric binding pocket of inactive $M_2$ (dark grey) and $M_4$ model (light grey). B: The EDGE-motif of $M_2$ AChR with three acidic residues is a unique motif for MAChRs C: In the $M_5$ AChR a glutamine can be found instead of an aromatic residue in the middle of EL2. D: EL2 and EL3 are connected by a salt bridge in the $M_3$ AChR.

## 4.2 Dualsteric ligand binding

For the $M_2$AChR, orthosteric, allosteric and dualsteric ligands are known [99, 101-103]. Dualsteric ligands are of particular interest because they combine the high affinity of orthosteric ligands with the subtype selectivity gained from the allosteric binding site. Recently published crystal structures of the $M_2$AChR [94, 95] and available mutational studies offer the possibility to rationalize dualsteric ligand binding on a structural level for the first time. The following paragraphs will focus on the ability of dualsteric ligands to fine-tune the receptor function in terms of subtype selectivity, partial agonism and biased signaling.

### 4.2.1 Rationalization of dualsteric binding modes

Our extensive MD simulations in combination with docking and 3D-pharmacophore analysis show that the concept of dualsteric binding can be rationalized [99]. Insights into the flexibility of the allosteric binding pocket confirm earlier hypotheses: A comparison of dualsteric ligands (Atr-6-phth (**10**), Sco-6-phth (**12**), Atr-6-naph (**11**) and Sco-6-naph (**13**)) highlights the crucial role of the tropane ring system for the arrangement of the allosteric moiety. Whereas EL2 mainly contributes to the binding of the Scopolamine-based hybrid structures, it only plays a minor role for the binding of Atropine-based ligands. Orthosteric ligand binding was similar for all ligands and characterized by an essential electrostatic interaction with D103 and an aromatic cage build by Y104, W400, Y403 and Y426. The crystal structure of the $M_2$ AChR with co-crystallized QNB (**1**) [94] offers a characterization of the orthosteric binding site, which mainly consists of aromatic residues. Y403 limits the orthosteric binding pocket towards the extracellular regions, where the allosteric binding site is located (Figure 24). The general ligand orientation is induced by D103 through electrostatic interaction with positively charged nitrogen, not only as observed with QNB (**1**) but also for Atropine (**3**) and Scopolamine (**4**) (as described in 4.1.1). Opposite to this hydrophilic region there are two lipophilic pockets. While the inverse agonist QNB (**1**) fills both regions with its two phenyl rings, the tropane alkaloids Atropine (**3**) and Scopolamine (**4**) just cover one cavity each, interestingly not the same (Figure 23). The preference of the phenyl ring for one of these lipophilic pockets is affected by the orientation of the tropane ring system. The additional epoxide group in Scopolamine (**4**) turns the tropane moiety in a different orientation for Atropine (**3**). Additionally, the epoxide group serves as a

hydrogen bond donor for the thiol group of C429 (Figure 16B). The different orientation of the tropane ring system results in different binding modes for the allosteric building blocks. While the allosteric modulation of Atropine-based hybrid structures depends on direct interaction with W422 (Figure 24A), the Scopolamine-based hybrid structures interact with Y177 of the EL2 (Figure 24B). These findings are in accordance with mutagenesis studies that indicate the Atropine-based ligands to be sensitive to the mutant $M_2$ W422A, whereas binding of the Scopolamine (**4**)-based ligands remains unaffected [99].

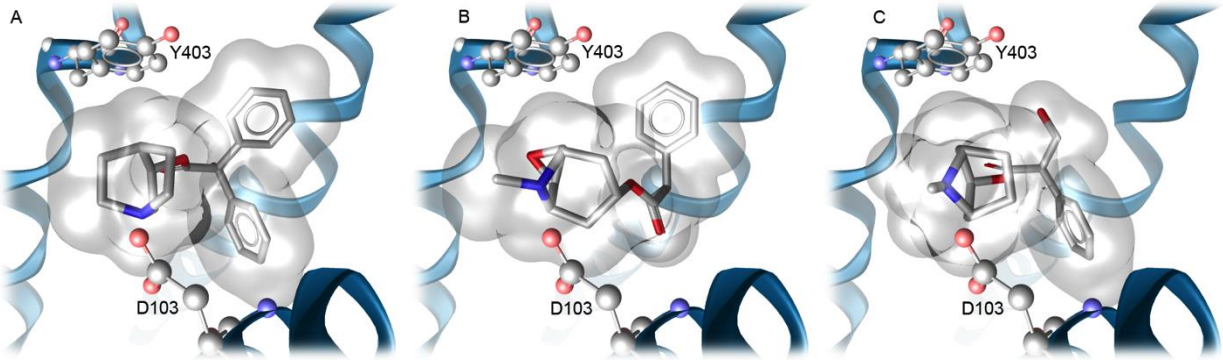


Figure 23: Binding mode comparison of the orthosteric ligands QNB (**1**) (A), Scopolamine (**4**) (B) and Atropine (**3**) (C) in the $M_2$AChR.

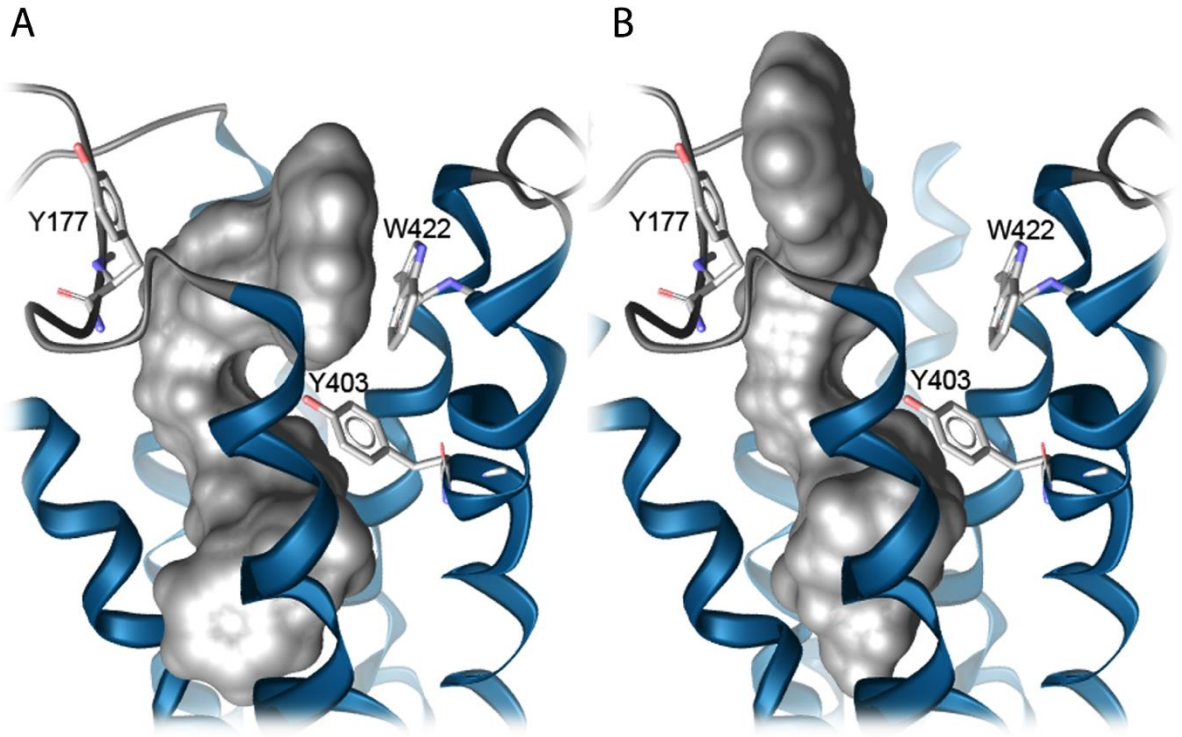


Figure 24: Molecular surfaces of Atr-6-naph (**11**) (A) and Sco-6-naph (**13**) (B) in the $M_2$AChR indicate a different arrangement of the allosteric part

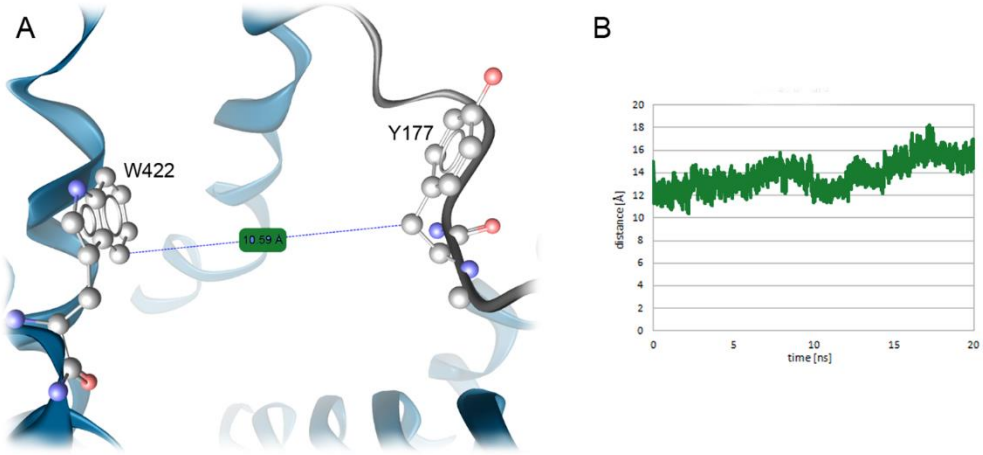


Figure 25: A: The crystal structure of the $M_2$AChR indicates a minimum distance of over 10 Å between Y177 of EL2 and W222 in the beginning of TM7. B: Minimum distance between Y177 and W422 during 20 ns simulation of the apo structure.

Extensive molecular dynamics simulations of dualsteric ligands (Atr-6-phth (**10**), Sco-6-phth (**12**), Atr-6-naph (**11**) and Sco-6-naph (**13**)) confirm the differences of the Atropine-based and Scopolamine-based hybrid structures in dualsteric binding derived from docking [99]. The general orientation of the allosteric part that results from the different orientation of the tropane moiety in the orthosteric part remains unchanged during 20 ns MD simulation for all ligands (Figure 26B, Figure 27B, Figure 28B and Figure 29B). However, 3D-pharmacophore analyses of the stable states unveil new interaction motifs for the dualsteric ligands (Figure 26A, Figure 27A, Figure 28A and Figure 29A). Y177 and W422 constitute the border of the allosteric binding pocket and are potentially capable for π-cation interactions with the positively charged nitrogen in the allosteric part of all the investigated ligands. Neither the former postulated direct π-π interaction between Y177 and W422, nor the π-π interactions of the allosteric ring systems with both Y177 and W422 [103] occur during the simulations. The distance between the allosteric epitopes Y177 and W422 can be used as an indicator for the flexibility of the allosteric vestibule [36]. Due to the constitutive activity this distance highly varies in the simulation of the apo-structure (Figure 25). In the simulations with hybrid structures this distance varies less and indicates a dualsteric binding mode with a stabilizing effect for the inactive receptor conformation (Figure 26C, Figure 27C, Figure 28C and Figure 29C). The connection of extracellular loops may enhance allosteric ligand binding. For Sco-6-naph (**13**), a connection of the extra-cellular loops 2 and 3 through π-cation interactions with the positively charged nitrogen in the allosteric ligand part can be observed. Atr-6-naph (**11**) that strongly interacts with EL3, also shows hydrophobic contacts to Y177 via the two methyl groups of the short aliphatic linker.

Orthosteric ligand binding occurs in a highly similar way for all known ligands and is characterized by an essential charge interaction with D103, while the orthosteric binding pocket is sterically constrained by an aromatic cage (see also chapter 4.1.1). In the following paragraphs the binding mode of the dualsteric ligands Atr-6-phth (10), Atr-6-naph (**11**), Sco-6-phth (**12**) and Sco-6-naph (**13**) will be described in detail with a focus on the allosteric interaction pattern.

*Atr-6-phth (**10**):* The allosteric building block of Atr-6-phth (**10**) strongly interacts with EL3 [99]. After 5 ns of simulation Atr-6-phth (**10**) reaches a stable conformation that unveils receptor-ligand interactions leading to a stabilized receptor conformation (Figure 26). The following interactions with the allosteric binding site are observed by 3D pharmacophore analysis and illustrated in Figure 26A: One carbonyl group of the phthalimide serves as hydrogen bond acceptor for T423, the other one as hydrogen bond acceptor for N410. The phthalimide builds up a π-π interaction with W422 and is embedded in a lipophilic pocket, consisting of W422 and A414. The positively charged nitrogen interacts with Y80, Y426 and W422 through π-cation interactions.

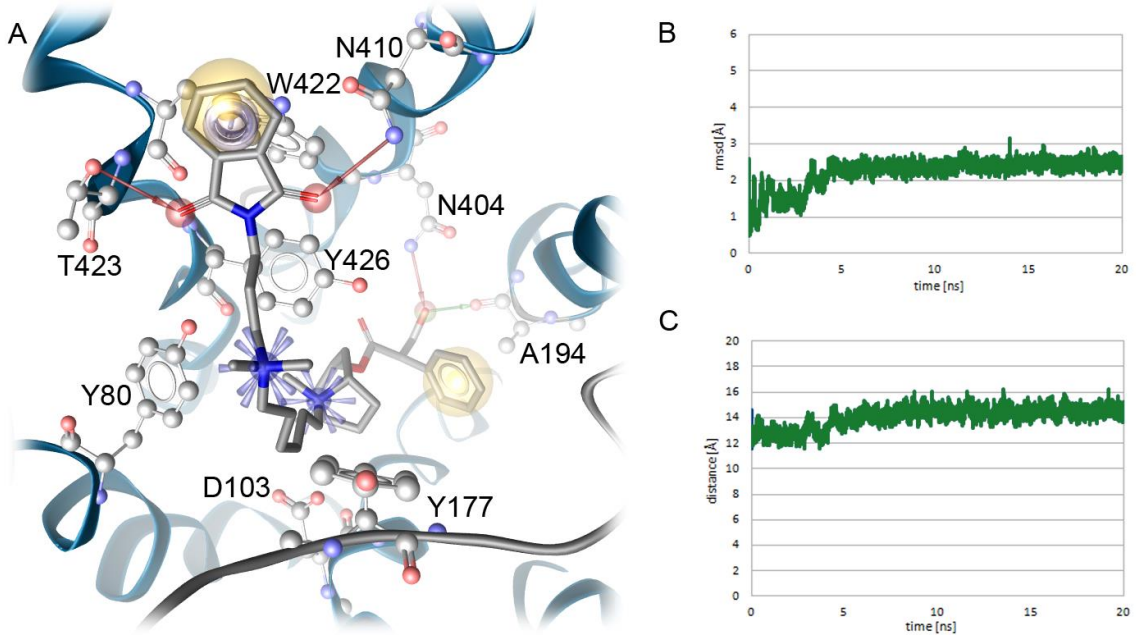


Figure 26: A: 3D pharmacophore analysis of Atr-6-phth (**10**) in the $M_2$AChR. Yellow spheres indicate lipophilic contacts, red arrows hydrogen bond acceptors, green arrows hydrogen bond donors, the purple disk represents a π-stacking interaction and positive ionazable centres are shown as blue spheres. B: overall geometry deviation of backbone atoms for 20 ns simulation Atr-6-phth (**10**). C: distance between Y177 and W422 during 20 ns simulation with bound Atr-6-phth (**10**).

*Atr-6-naph (**11**):* The allosteric part of Atr-6-naph (**11**) is mainly oriented towards EL3 [99]. After 7 ns of simulation Atr-6-naph (**11**) reaches a stable conformation that indicates receptor-ligand interactions leading to a stabilized receptor conformation (Figure 27). The following interactions with the allosteric binding site are observed by 3D pharmacophore analysis. One carbonyl group of the allosteric ring system serves as hydrogen bond acceptor for N419, the other one as hydrogen bond acceptor for Y426. The ring system is opposite W422 and A414 and the two methyl groups of the short aliphatic linker are embedded in a lipophilic pocket, built by Y177. The positively charged nitrogen interacts through π-cation interactions with Y80, Y426 and W422.

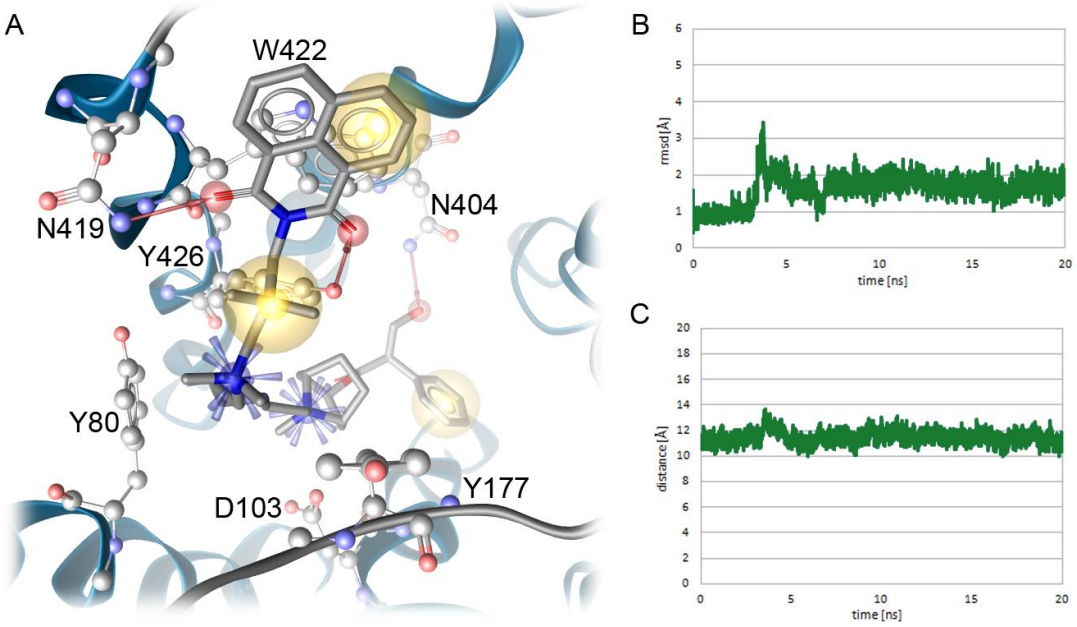


Figure 27: A: 3D pharmacophore analysis of Atr-6-naph (**11**) in the $M_2$AChR. Yellow spheres indicate lipophilic contacts, red arrows hydrogen bond acceptors and positive ionazable centres are shown as blue spheres. B: overall geometry deviation of backbone atoms for 20 ns simulation Atr-6-naph (**11**). C: distance between Y177 and W422 during 20 ns simulation with bound Atr-6-naph (**11**).

*Sco-6-phth (**12**)*: The allosteric building block of Sco-6-phth (**12**) is positioned opposite of Y177 of the EL2 [99]. During the first 2 ns of simulation Sco-6-phth (**12**) reaches a stable conformation that unveils receptor-ligand interactions leading to a stabilized receptor conformation (Figure 28). The following interactions with the allosteric binding site are observed by 3D pharmacophore analysis: The phthalimide is opposite Y177 of the EL2 and builds up a π-π interaction with this tyrosine. The positively charged nitrogen interacts through π-cation interactions with Y83, Y426 and W422.

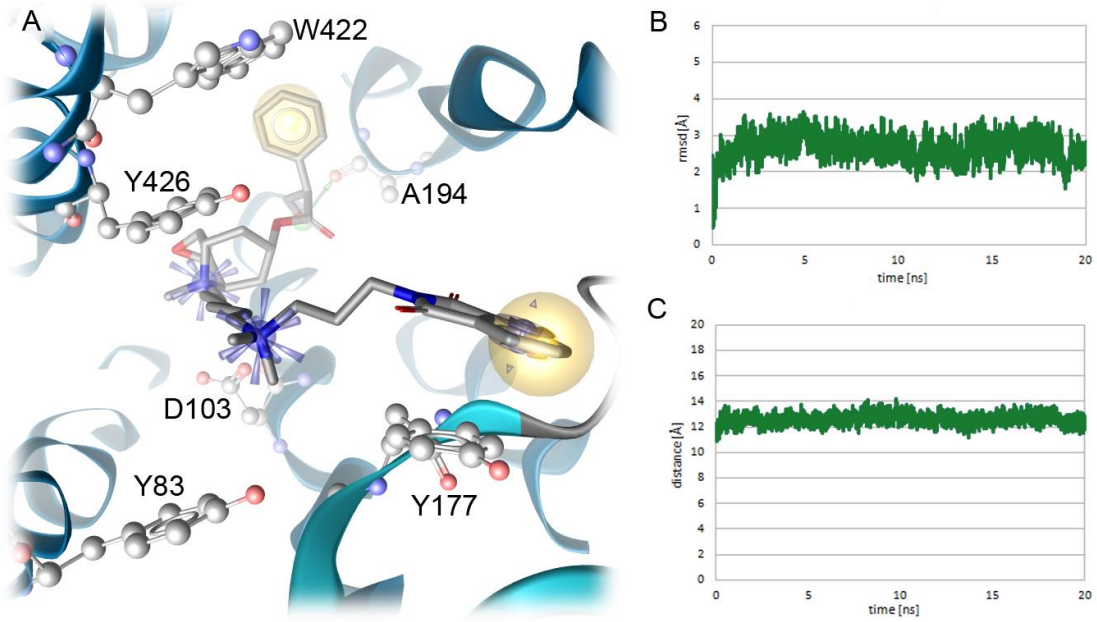


Figure 28: A: 3D pharmacophore analysis of Sco-6-phth (**12**) in the $M_2$AChR. Yellow spheres indicate lipophilic regions, green arrows hydrogen bond donors, the purple disk represent a π-stacking interaction and positive ionazable centres are shown as blue spheres. B: overall geometry deviation of backbone atoms for 20 ns simulation Sco-6-phth (**12**). C: distance between Y177 and W422 during 20 ns simulation with bound Sco-6-phth (**12**).

*Sco-6-naph (**13**):* The allosteric part of Sco-6-naph (**13**) is mainly oriented towards EL2 [99]. The following interactions with the allosteric binding site are observed by 3D pharmacophore analysis and are taken from a representative frame of the last two ns of MD simulation (Figure 29A). The 1,3-dioxo-1H,3H-benzo(de)isoquinoline is positioned opposite to Y177, which is also part of a lipophilic pocket binding the two methyl groups of the short aliphatic linker. The positively charged nitrogen interacts through π-cation interactions with Y83, Y177 and W422.

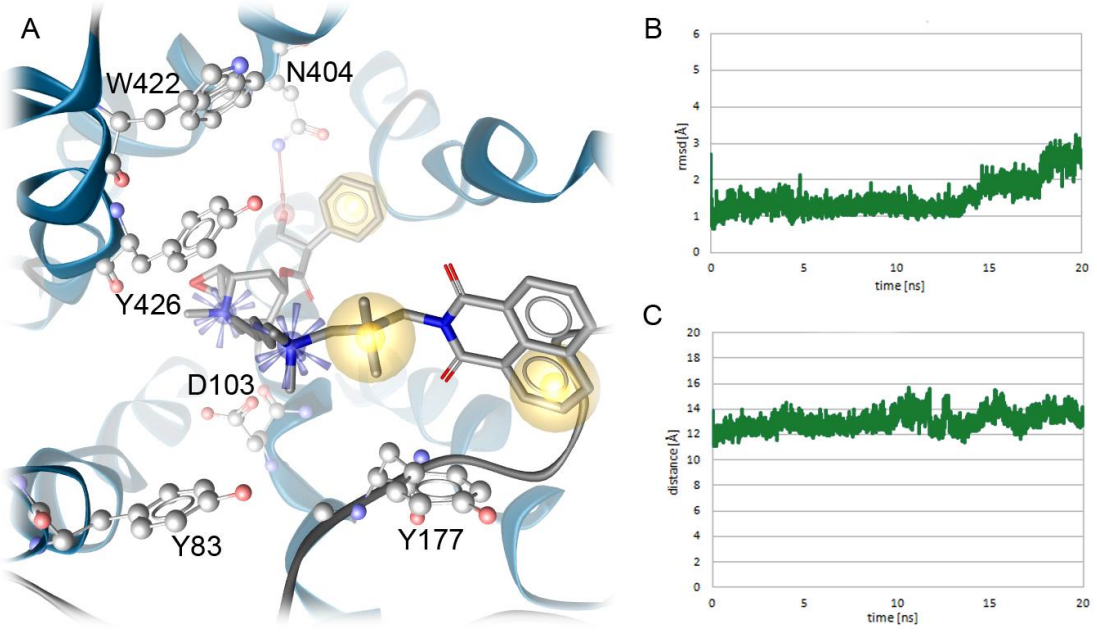


Figure 29: A: 3D pharmacophore analysis of Sco-6-naph (**13**) in the $M_2$AChR. Yellow spheres indicate lipophilic regions, red arrows hydrogen bond acceptors and positive ionazable centres are shown as blue spheres. B: overall geometry deviation of backbone atoms for 20 ns simulation Sco-6-naph (**13**). C: distance between Y177 and W422 during 20 ns simulation with bound Sco-6-naph (**13**).

Interestingly, 20 ns simulation of Sco-6-naph (**13**) bound to the $M_2$ AChR shows three different states for the position of the allosteric ring system. For the first 12 ns the 1,3-dioxo-1H,3H-benzo(de)isoquinoline allows for a π-π interaction with Y177 (Figure 30A). In that conformation the aliphatic linker, connecting the orthosteric with the allosteric building block is buckled. After 12 ns the aliphatic linker is stretching resulting in a movement of the allosteric ring system with an intermediate state during 15 and 18 ns (Figure 30B), before finally re-orienting the allosteric ring system (Figure 30C). This rearrangement of the allosteric molecule part is further illustrated in Figure 31.

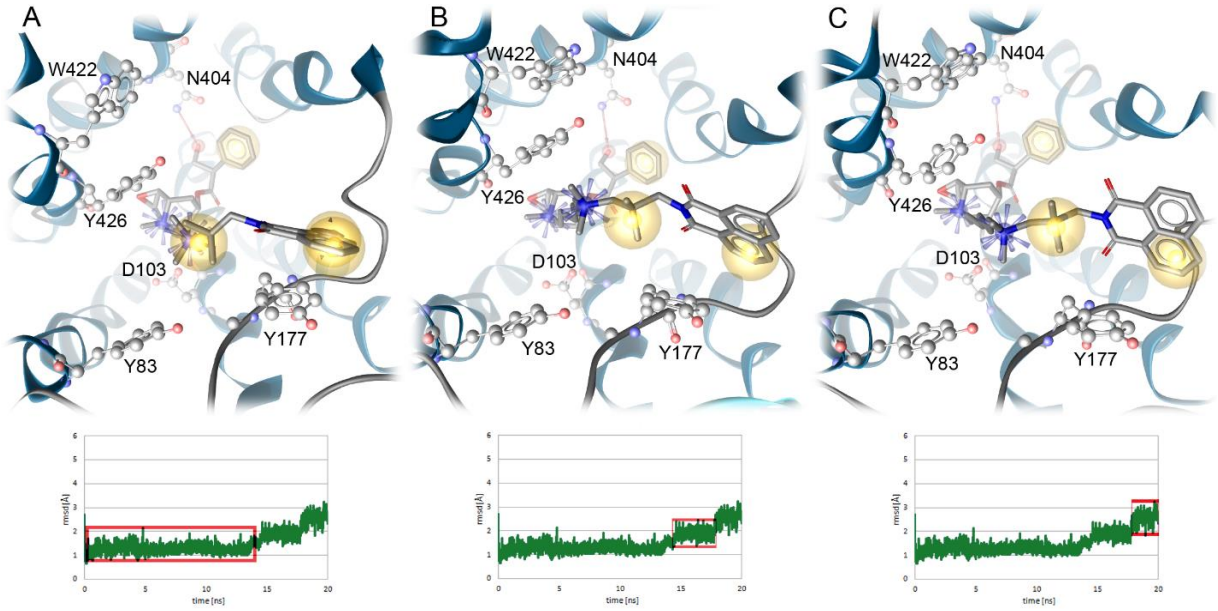


Figure 30: 3D pharmacophore analysis of the three representative states of Sco-6-naph (**13**) in the $M_2$AChR for Sco-6-naph (**13**) during the first 12 ns (A), after stretching in the intermediate state (B) and in the final state (C). Yellow spheres indicate lipophilic regions, red arrows hydrogen bond acceptors, the purple disk represents a π-stacking interaction and positive ionazable centres are shown as blue spheres.

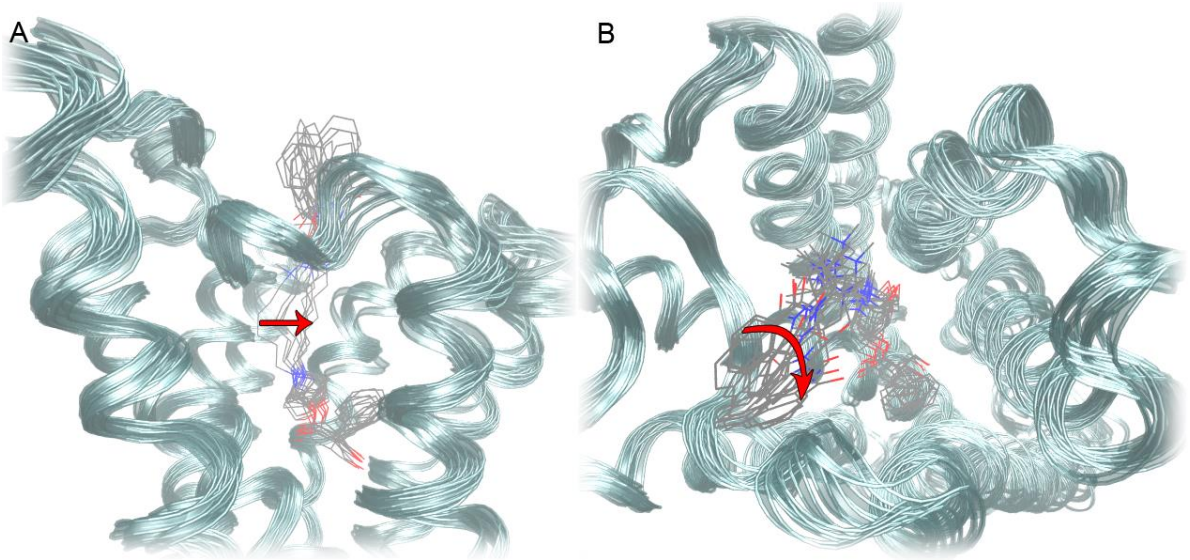


Figure 31: During the simulation the aliphatic linker in Sco-6-naph (**13**) stretches (A), which results in a slight spin of the allosteric ring system (B).

### 4.2.2 Subtype selectivity of dualsteric ligands

In the modeling part that we contributed to Schmitz et al. [99] we characterized the dualsteric binding mode of hybrid structures binding to the $M_2$AChR. Dualsteric ligand binding was shown to reach a $M_2$ over $M_5$ selectivity for several ligands (e.g. Iper-6-phth (**15**) and Atr-6-naph (**11**)). The derived homology models of $M_5$ AChR allow a rational explanation of the measured selectivity for the first time [36]. Docking experiments in combination with 3D pharmacophore model analyses performed within the scope of this thesis unveiled the structural basis for the subtype selectivity of dualsteric ligands on two examples: Iper-6-phth (**15**) and Atr-6-naph (**11**) [36].

The first example gives an explanation for the $M_2$ over $M_5$ selectivity of the dualsteric agonist Iper-6-phth (**15**). The orthosteric building block of the dualsteric agonist Iper-6-phth (**15**) indicates similar receptor-ligand interactions for $M_2$AChR and $M_5$AChR, whereas the interaction pattern for the allosteric moieties differ (Figure 32). In the $M_2$AChR receptor the aromatic ring system of Iper-6-phth (**15**) is embedded between Y177 (Figure 32A) and A414, while in $M_5$AChR it is located opposite to L162 that corresponds to $M_2$ F181 (Figure 32B). The positive ionazable nitrogen in the allosteric linker shows π-cation interactions with W422 and Y83 in $M_2$ and the corresponding residues in $M_5$. Additionally, it forms an electrostatic interaction with E175 in the $M_2$ AChR. W231 of the $M_5$ receptor forms a hydrogen bond with a carbonyl group of the phthalimide moiety.

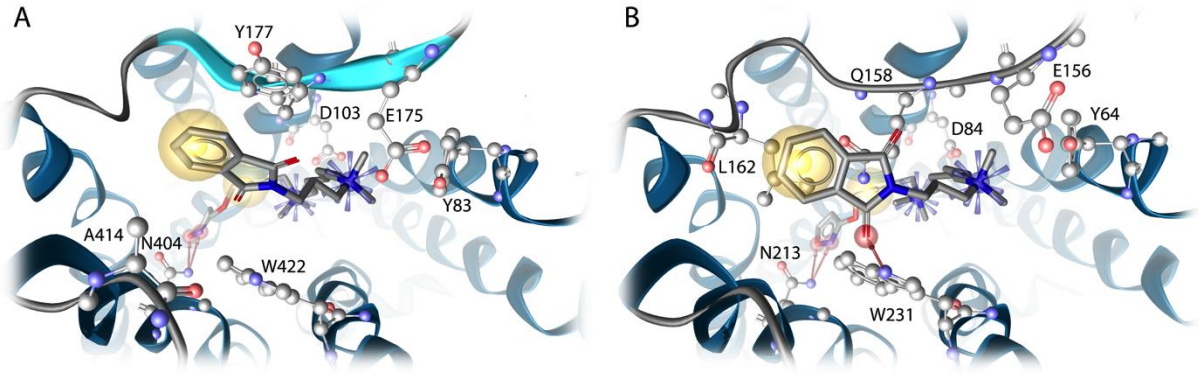


Figure 32: 3D-pharmacophores analysis of the dualsteric agonist Iper-6-phth (**15**) (A: $M_2$ receptor; B: $M_5$ receptor). Yellow spheres indicate lipophilic contacts, red arrows hydrogen bond acceptors and positive ionazable centers are shown as blue spheres.

The second example clarifies the different binding modes of Atr-6-naph (**11**) in $M_2$ (Figure 33A) and $M_5$ AChR (Figure 33B). Similar to the dualsteric agonist Iper-6-phth (**15**), no significant binding mode changes can be seen for the orthosteric part. In the $M_2$ AChR N419 and Y426 are forming hydrogen bonds with the carbonyl groups of the allosteric building block. Due to a valine in the position of $M_2$ N419 and a different orientation of the allosteric ring system, the $M_5$ AChR lacks these interactions. The allosteric ring system of Atr-6-naph (**11**) is situated opposite to $M_2$ W422/$M_5$ W231 but shows additionally hydrophobic contacts with $M_5$ V226. The short aliphatic linker that contains two methyl groups is opposite to $M_2$ Y177, but indicates no interactions with EL2 in the $M_5$ AChR. Taken together, the allosteric building block of Atr-6-naph (**11**) unveils several interactions with residues of EL3/TM7 but also with Y177 (EL2) in the $M_2$ AChR, but misses this connection of EL2 and EL3 in the $M_5$ AChR.

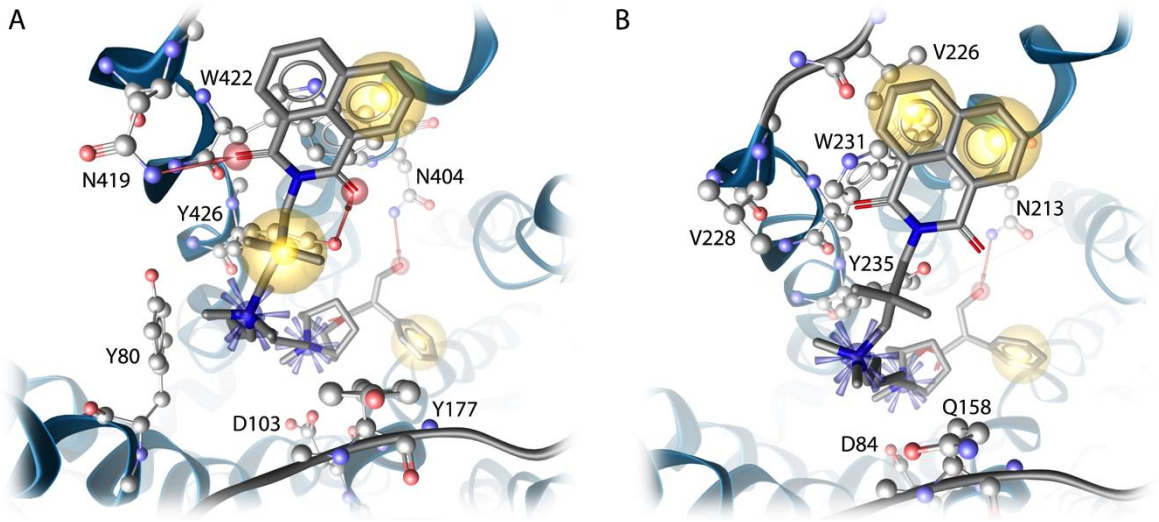


Figure 33: 3D-pharmacophores analysis of Atr-6-naph (**11**) (A: $M_2$ AChR; B: $M_5$ AChR). Yellow spheres indicate lipophilic contacts, red arrows hydrogen bond acceptors and positive ionazable centers are shown as blue spheres.

The dualsteric ligands are both able to connect EL2 and EL3 in the $M_2$ AChR subtype, but not in the $M_5$ AChR. Therefore Iper-6-phth (**15**) and Atr-6-naph (**11**) may enhance the stabilization of specific receptor conformations of the $M_2$ AChR, but are insufficient for the same effect in $M_5$ AChR, which leads to $M_2$ over $M_5$ AChR selectivity.

### 4.2.3 Partial agonism by dynamic ligand binding

As described in section 4.2.1, dualsteric ligands simultaneously bind to the orthosteric and the allosteric site, which results in a high binding affinity and offers the possibility to gain subtype selectivity [99]. The binding of a ligand leads to a stabilization of specific receptor conformations from a larger ensemble and facilitates specific receptor functions. Therefore it is not mandatory that only one binding conformation exists. It was first shown for estrogen receptors that one ligand can bind differently to the active and inactive conformation of the receptor [104]. This concept can be transferred to other protein classes, also MAChRs. Bock et al. [105] reported the coexistence of two functionally distinct populations of the $M_2$ AChR that are stabilized by one ligand. The switch between two functionally different binding modes, results in active and inactive receptor conformations. This so-called *dynamic ligand binding* represents a novel concept of partial agonism and allows controlling of ligand efficacy [105]. The combination of docking experiments and MD simulations confirmed this new concept and elucidated the different binding modes as a structural basis for partial agonism, taking the $M_2$ AChR as example.

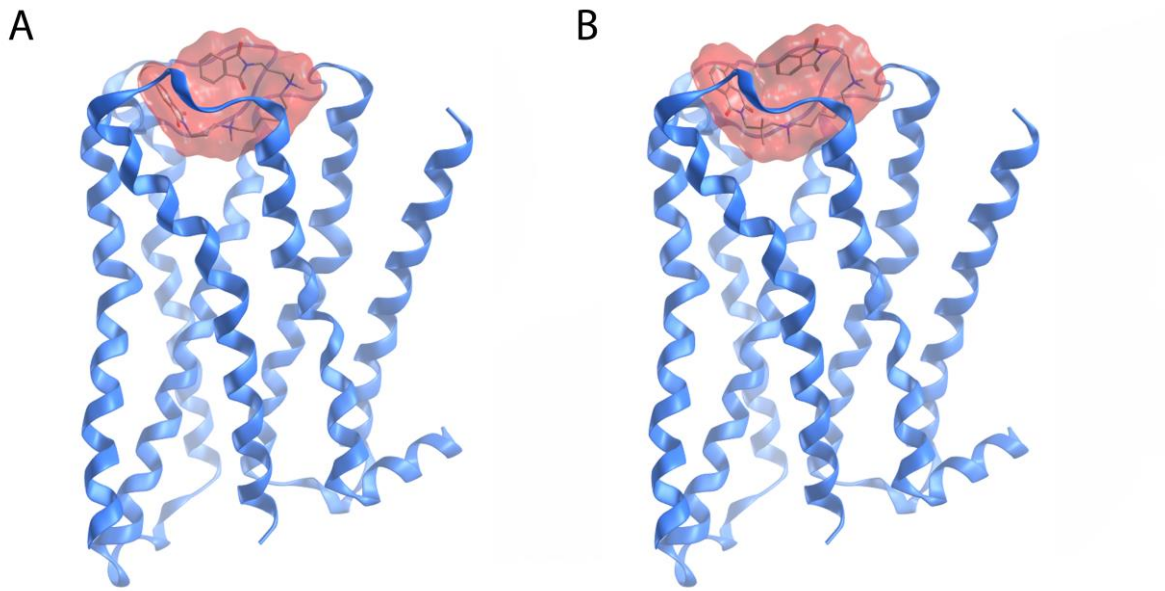


Figure 34: Binding site location for purely allosteric modulators W84 (**8**) and Naphmethonium (**9**).

The ability of orthosteric/allosteric hybrid ligands to bind in a dualsteric manner, occupying the orthosteric and the allosteric binding site simultaneously, was previously shown by our modeling study reported in Schmitz et al. [99] (see chapter 4.2.1). In addition to dualsteric ligand binding, the receptor allows for an alternative binding mode in the extracellular region, comparable to purely allosteric binders like W84 (**8**) (Figure 34A) or Naphmethonium (**9**) (Figure 34B) [106]. This variability of ligand binding results in the stabilization of two different receptor states: active (dualsteric ligand binding) and inactive (allosteric ligand binding). In this study, the dualsteric agonists Isox-6-naph (**14**), Iper-6-naph **(16)** and Iper-8-naph (**17**) were investigated in terms of dynamic ligand binding. Whereas the dualsteric binding mode of these ligands was similar (Figure 35A, Figure 36A and Figure 37A), they unveiled differences in their allosteric binding mode. The allosteric binding location of the hybrid structures with a linker chain length of six carbon atoms (Isox-6-naph (**14**) and Iper-6-naph **(16)**) was situated deeper in the receptor (Figure 35B and Figure 36B). Iper-8-naph (**17**) persists on the extracellular side and was unable to enter the transmembrane core region (Figure 37B).

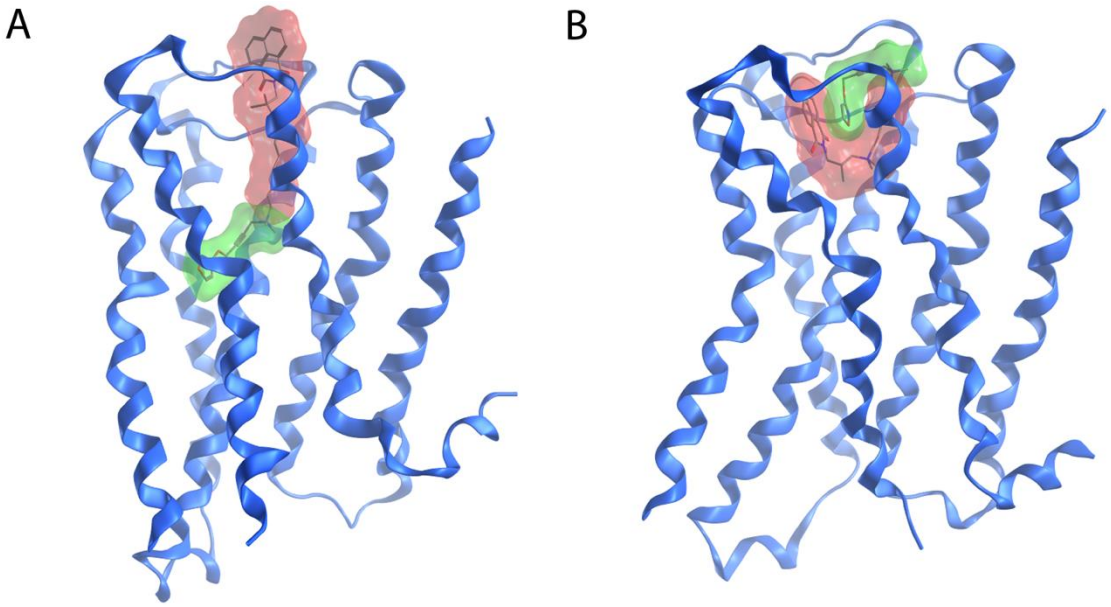


Figure 35: Dynamic ligand binding of Isox-6-naph (**14**) indicate two different binding modes, dualsteric (A) and allosteric (B).

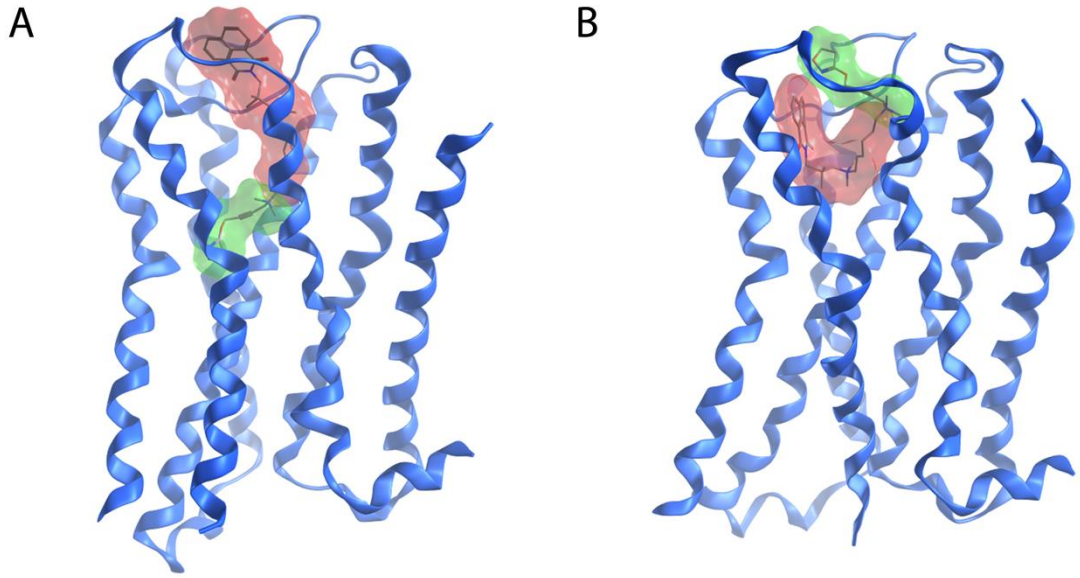


Figure 36: Dynamic ligand binding of Iper-6-naph (**16**) indicate two different binding modes, dualsteric (A) and allosteric (B).

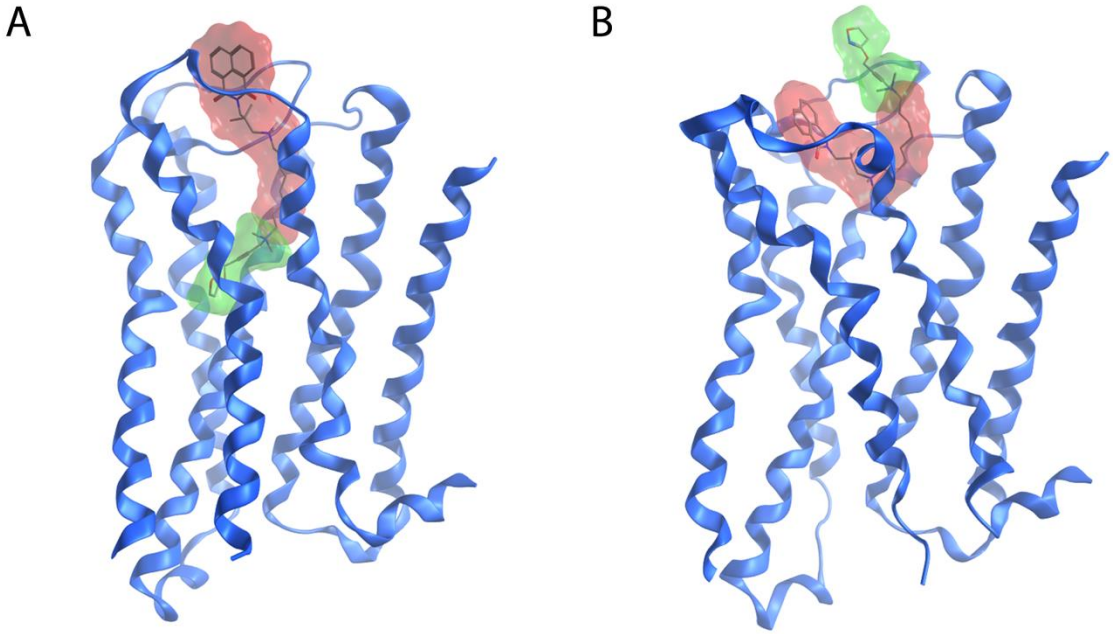


Figure 37: Dynamic ligand binding of Iper-8-naph (**17**) indicate two different binding modes, dualsteric (A) and allosteric (B).

In order to confirm the allosteric binding mode of the agonistic hybrid structures, MD simulations were carried out. These simulations give a reasonable explanation for the different pharmacological properties of the investigated ligands. Whereas Iper-8-naph (**17**) was shown to be a full agonist, Iper-6-naph (**16**) and Isox-6-naph (**14**) could be classified as partial agonists [105]. The MD simulation unveiled no stable binding mode for Iper-8-naph (**17**) in the allosteric orientation (Figure 38C), which can be interpreted as the disability of Iper-8-naph (**17**) to stabilize an inactive receptor state. Despite its flexibility, the C-8 chain is to long for allosteric ligand binding. Therefore, Iper-8-naph (**17**) may only stabilize the active receptor conformations through dualsteric binding, which results in full agonistic binding properties.

In contrast, Isox-6-naph (**14**) (Figure 38A) and Iper-6-naph (**16**) (Figure 38B) remain stable in the allosteric binding pocket. Therefore they show both, allosteric and dualsteric binding properties. Interestingly, the resulting partial agonistic activities are different. The higher efficacy of Iper-6-naph (**16**) compared with Isox-6-naph (**14**) can be illustrated by the quantification of the fractional receptor occupancy. Whereas Iper-6-naph (**16**) shows a pronounced preference for the dualsteric binding mode (79% versus 21%), Isox-6-naph (**14**) only binds in the dualsteric conformation to a small extent (7% versus 93%) [105].

The question arises, why Isox-6-naph (**14**) has such a high preference for the allosteric binding mode. A closer look to the receptor-ligand interactions unveil that both carbonyl groups of Isox-6-naph (**14**) can serve as hydrogen bond acceptors for Y403 and I178. The allosteric key residue Y177 shows hydrophobic contacts with both the allosteric ring system and the triple bond of the Iperoxo (**5**) part. Previous mutational studies [100] showed that E175 of the EDGE-sequence can be involved in ligand binding. This glutamic acid allows for electrostatic interaction with the positively charged nitrogen of the Iperoxo (**5**) moiety. Additionally, a very interesting intramolecular interaction can be observed for Isox-6-naph (**14**): The isoxazole ring is able to form a π-π interaction with the allosteric moiety. This intramolecular interaction stabilizes a conformation of Isox-6-naph (**14**) that is likely to bind to the allosteric vestibule. Taken together, this strong interaction pattern makes Isox-6-naph (**14**) to bind preferably in the allosteric pose and stabilizes inactive receptor conformations.

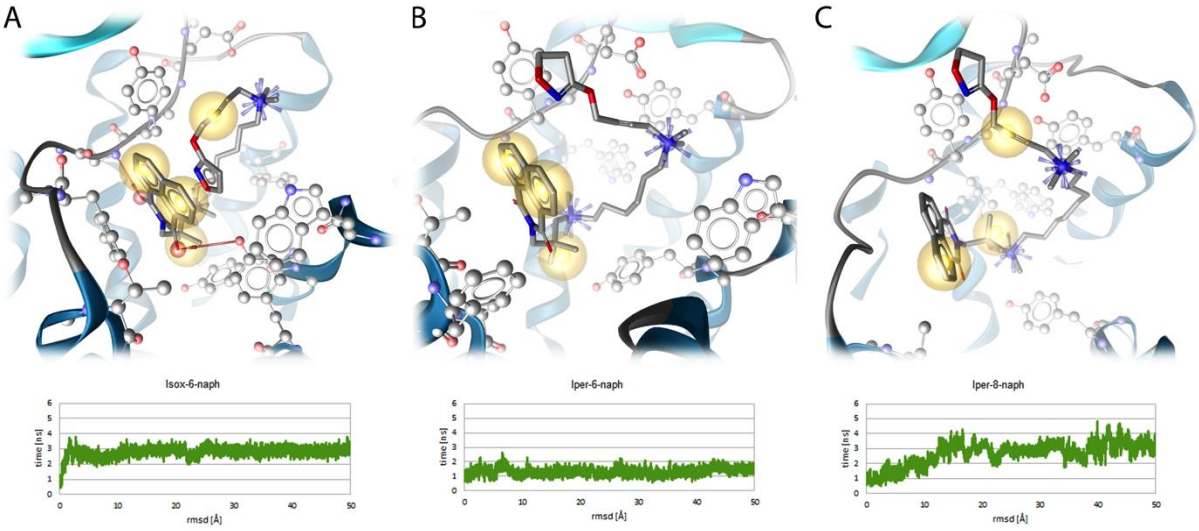


Figure 38: Allosteric binding modes for Isox-6-naph (**14**) (A), Iper-6-naph (**16**) (B) and Iper-8-naph (**17**) (C) and the overall geometry deviation of backbone atoms over 50 ns of MD simulation. Yellow spheres indicate hydrophobic contacts, red arrows hydrogen bond acceptors and positive ionazable centers are shown as blue spheres.

### 4.2.4 Signaling bias of dualsteric ligands

The Iperoxo-based hybrid ligands Iper-6-naph (**16**) (Figure 36) and Iper-8-naph (**17**) (Figure 37) were investigated in terms of their binding mode and their influence on the conformational space of the allosteric binding site, which may result in a distinct signaling repertoire [98]. Extensive molecular dynamics simulations of receptor-ligand complexes proved the dualsteric binding mode of these agonistic ligands (Figure 39B/C, Figure 40B/C). A closer look to the crystal structure of $M_2$ AChR bound to Iperoxo (**5**) [32] indicate key interactions for orthosteric ligand binding, such as an electrostatic interaction of D103 with a positively ionazable nitrogen or the formation of hydrogen bonds with N404. The orientations of the orthosteric building blocks of the investigated ligands were similar to Iperoxo (**5**) in the crystal structure and the above mentioned key interactions were found in all frames of the trajectories. Due to the fixed position of the Iperoxo (**5**) moiety in the orthosteric binding site, the chain length of the aliphatic linker strongly influences the interaction pattern of the allosteric building block. 3D-pharmacophore analysis of representative receptor-ligand complexes unveiled the differences in allosteric binding (Figure 39E/F, Figure 40E/F). The positively charged nitrogen of the allosteric part of Iper-6-naph (**16**) forms a π-cation interaction with Y426. The aromatic ring system of Iper-6-naph (**16**) lies opposite to Y177, which allows for a π-π-interaction. The binding mode of Iper-8-naph (**17**) reveals hydrophobic contacts of the allosteric ring system with A414 The positively charged nitrogen of the allosteric part of Iper-8-naph (**17**) forms a π-cation interaction with W422 and allows for an electrostatic interaction with E175.

The different interaction pattern of the two described dualsteric agonists result from the different length of the linker chain. Whereas the allosteric ring system of Iper-8-naph (**17**) sticks out of the extracellular domains it is located closer to the orthosteric binding site for Iper-6-naph (**16**). Therefore they influence the conformational flexibility of the extracellular domains differently, which has consequences on the signaling repertoire. The activation of a GPCR is characterized by conformational changes that expose intracellular epitopes for the interaction with signaling proteins. Besides a basal activity, these changes of the receptor conformation are driven by ligands that can stabilize a distinct activation state.

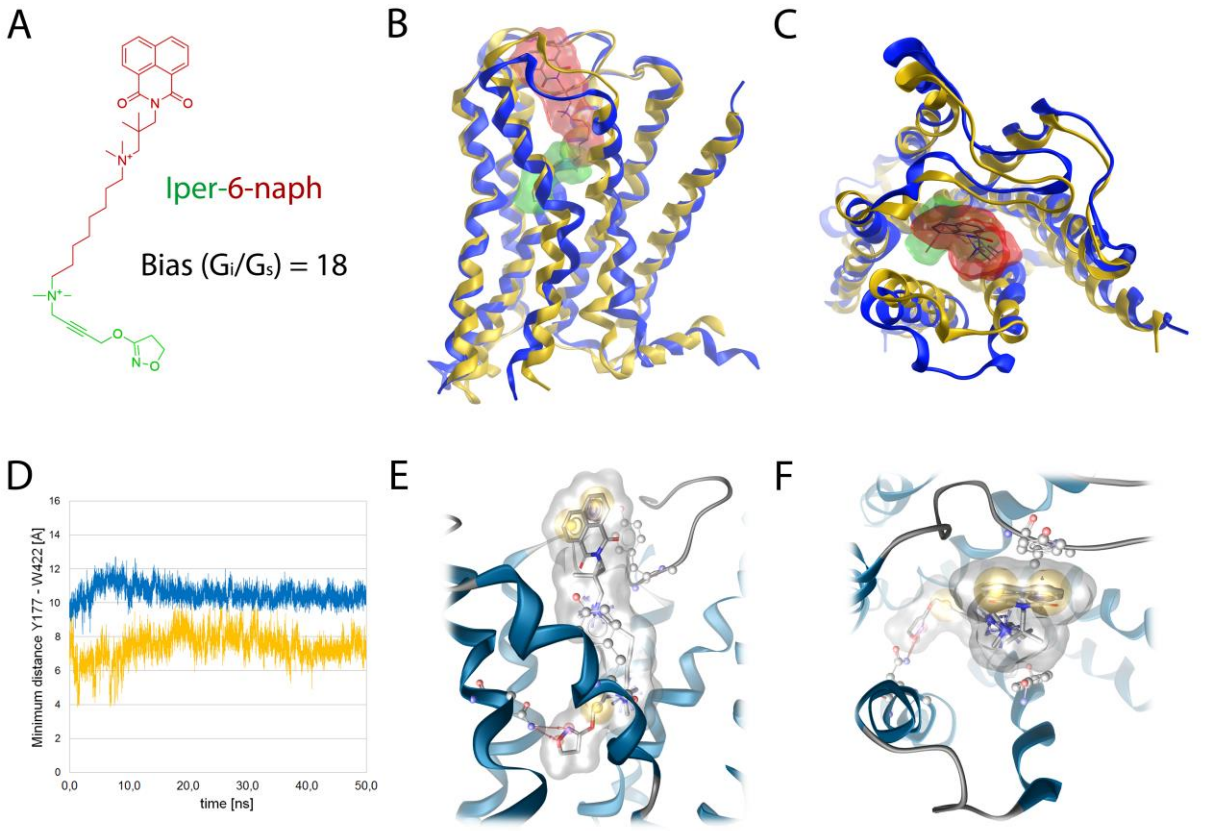


Figure 39: Binding mode characterization of Iper-6-naph (**16**) in the $M_2$ receptor. The orthosteric part is shown in green and the allosteric part in red (A-C). (A): 2D-representation of Iper-6-naph (**16**); (B/C) Dualsteric binding mode of Iper-6-naph (**16**) in the $M_2$ receptor (blue). A representative receptor conformation with Iperoxo (**5**) is superimposed for a comparison (yellow). (D): Minimum distance between Y177 and W422 during the MD simulation of the $M_2$ AChR bound to Iper-6-naph (**16**) (blue) and Iperoxo (**5**) (yellow). (E/F): 3D pharmacophore analysis of Iper-6-naph (**16**), Yellow spheres indicate lipophilic contacts, red arrows hydrogen bond acceptors, the purple disk represents a π-stacking interaction and positive ionazable centres are shown as blue spheres.

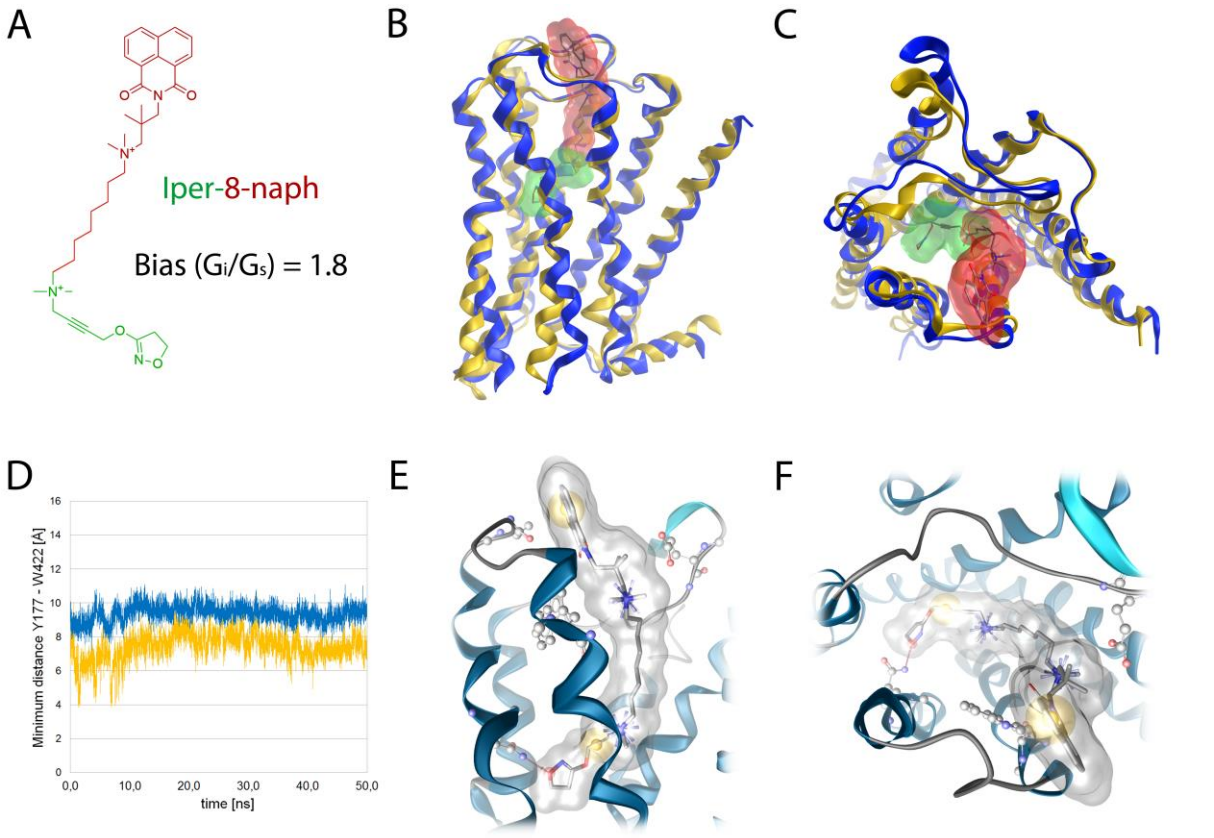


Figure 40: Binding mode characterization of Iper-8-naph (**17**) in the $M_2$ receptor. The orthosteric part is shown in green and the allosteric part in red (A-C). (A): 2D-representation of Iper-8-naph (**17**); (B/C) Dualsteric binding mode of Iper-8-naph (**17**) in the $M_2$ receptor (blue). A representative receptor conformation with Iperoxo (**5**) is superimposed for a comparison (yellow). (D): This graph shows the minimum distance between Y177 and W422 during the MD simulation of the $M_2$ AChR bound to Iper-8-naph (**17**) (blue) and Iperoxo (**5**) (yellow). (E/F): 3D pharmacophore analysis of Iper-8-naph (**17**), Yellow spheres indicate lipophilic contacts, red arrows hydrogen bond acceptors and positive ionazable centres are shown as blue spheres.

Comparisons of crystal structures in activated/inactivated form (PDB: 4MQS [32] and 3UON [94]) show that the allosteric vestibule narrows during activation while the intracellular side enlarges [32, 94]. Therefore allosteric ligands as well as the allosteric part of dualsteric ligands are able to regulate the activation process by enhancing or blocking the above mentioned conformational changes.

Multiple signaling roles of GPCRs indicate that there is no general activation mode. In fact, GPCRs prefer a distinct profile of signaling cascades [36] that can be modulated in a ligand-dependent manner. Molecular dynamics simulations of the dualsteric agonists Iper-6-naph (**16**) and Iper-8-naph (**17**) unveil that the allosteric moieties control the conformational rearrangement of the allosteric binding site. This restriction of conformational space makes the receptor incapable of performing its entire signaling repertoire. Whereas the superagonist Iperoxo (**5**) allows for the exhaustive closure of the extracellular domains, the allosteric building blocks hamper this conformational rearrangement (Figure 39D, Figure 40D).

Iper-8-naph (**17**) shows a slight $G_i$ bias [98], which is in accordance with the structural model. A structural comparison of the extracellular region shows that the allosteric binding site is wider for the Iper-8-naph (**17**) bound receptor than in the Iperoxo-bound complex. Due to the deeper orientation of the allosteric ligand part in the Iper-6-naph (**16**)-bound receptor, the extracellular closure is hampered to a larger extent, compared to Iper-8-naph (**17**). Therefore, the $G_i$ bias of Iper-6-naph (**16**) is 10-fold stronger than for Iper-8-naph (**17**) [98]. For the application of MD simulations, the distance between the previously described key epitopes Y177 and W422 [36, 99] can serve as an indicator for the structural characteristics of the allosteric vestibule and can therefore be used as a surrogate parameter for biased signaling. Taken together, the dualsteric agonists Iper-6-naph (**16**) and Iper-8-naph (**17**) show biased signaling with different quantities of $G_i$ bias depending on the chain length of the aliphatic linker.

# 5 Discussion

Structural and functional investigations of GPCRs are highly important and interesting, but also challenging. The absence of crystal structures for most GPCRs represents an obstacle for structure-based approaches. However, the combination of several computational methods and experimental data can enable medicinal chemists to build mechanistic models with high explanatory power [1]. Following this approach, homology models of all subtypes of MAChR could be developed and validated in the course of this thesis. These models can be used to unveil the structural basis of dualsteric ligand binding, which provides the possibility to modulate GPCR signaling using designed ligands in a predictable way.

## 5.1 Structural models of MAChR

The reported homology models of all five MAChR subtypes in their inactive and active-like conformations provide valuable information about the structural characteristics of a group of closely related receptors. Carefully conducted molecular dynamics simulations provided refined models and allowed for conformational sampling of the respective receptor subtypes.

As expected, all inactive receptor states showed a wide extracellular vestibule. This region consists of multiple epitopes that are involved in allosteric receptor modulation. Compared with the inactive conformations, the allosteric vestibule was narrow in all active-like receptor models, which is in accordance with other known crystal structures and the general activation model. The results of conformational sampling confirm the assumption of conformational rigidity of the transmembrane domains and illustrate the already assumed high flexibility of the extracellular loops [36]. Furthermore, a correlation between structural characteristics and functional properties were found. The distance b $M_2$ Y177 and $M_2$ W422 serves as structural descriptor that can distinguish between the preferences for $G_i$ or $G_q$ coupling. Receptor subtypes preferring $G_i$ coupling ($M_2$ and $M_4$ AChR) show a larger distance between these allosteric key residues. Our findings support the idea of an allosteric rearrangement that structurally imprints the receptor functionality upon activation.

The high conservation of the orthosteric binding pocket enables a broad diversity of chemical entities for binding to MAChRs. Ligand binding is characterized by an electrostatic key interaction of a positively ionazable center and an aspartic acid ($M_2$ D103). Additionally two lipophilic pockets allow structures that are larger than the physiological ligand acetylcholine to bind to the orthosteric site. Although these two pockets are not mandatory for acetylcholine binding, they have persisted evolutionary pressure. Hence, the assumption that unknown physiological ligands might exist, seems likely. The ability of the orthosteric binding site to host chemically diverse ligands has a major impact on medicinal chemistry. First, plenty of marketed drugs bind to MAChRs, mostly as inverse agonists or antagonists. The resulting anticholinergic side effects represent a major problem for the clinical use of a lot of known drugs, especially CNS-active drugs. The binding mode of three psychoactive drugs (Promethazine (**18**), Amitriptyline (**19**) and Clozapine (**20**)) was found to be very similar compared with the co-crystallized ligands QNB (**1**) and Tiotropium (**2**). Furthermore, the shown ligand binding promiscuity of the orthosteric binding site has to be considered also for pharmacological tools: NSC23766 (**6**) is widely used as inhibitor for RAC1, but was found to additionally bind to MAChRs in an unselective manner [48]. This example nicely shows that anticholinergic effects not only occur in clinical use, but also as an artifact for *in vitro* experiments. The reported structural models are suitable starting points to investigate unwanted binding effects for MAChRs and could serve as off-target models for rational drug design approaches.

A comparison of the derived homology models unveil structural characteristics for the five MAChR subtypes [36]. As mentioned before, the orthosteric binding site is highly conserved. Only marginal structural differences could be observed and only concern side chain orientations and different residues with the same chemical functionality. This explains the low subtype selectivity for most MAChR ligands. However, the extracellular domains represent an additional binding site and allow for allosteric modulation. The differences in the amino acid sequence of the five MAChR subtypes are reflected by different structural properties of this allosteric binding site. Hence, these structural characteristics can be investigated by using the homology modelling and offer the possibility to find anchor points for subtype selectivity. Some examples of unique structural motifs were found in the reported models. In the $M_2$AChR, the EDGE-

motif represents a unique cluster of negatively ionazable residues. Especially, E175 can form electrostatic interactions with possible ligands and may contribute to subtype selectivity. In the $M_3$ACHR, a salt bridge formed by $M_3$ E219 and $M_3$ K522 connects EL2 with EL3. This connection was observed in the inactive crystal structure but also in the active-like model. Allosteric modulation usually goes along with a connection of EL2 and EL3 bridged by a single ligand. Due to this salt bridge, the allosteric modulation of the $M_3$AChR might be restricted. Similar to the allosteric key residue $M_2$ Y177, aromatic amino acids in this position are present in all other subtypes, except $M_5$ AChR. Hence, allosteric binders for $M_5$ AChR are unable to form π-π or π-cation interactions in this region. However, the glutamine residue in this position allows for hydrogen bonding with possible ligands. The reported structural characteristics provide a starting point for the rational design of subtype selective MAChR modulators.

Taken together, our results illustrate the high impact of carefully developed and structurally refined homology models for the investigation of MAChRs. The application of homology modeling in combination with MD simulations represents a suitable modeling strategy, also for other GPCR targets with unresolved crystal structures.

## 5.2 Dualsteric ligand binding

The concept of dualsteric ligand binding combines the high affinity for the orthosteric binding pocket with the subtype selectivity gained from the allosteric binding site. In order to explore and mechanistically explain this concept of simultaneous binding to different binding sites, the binding modes of dualsteric ligands were investigated in the $M_2$AChR. For this attempt, first docking experiments were carried out to obtain suitable binding poses. To evaluate the generated binding modes MD simulations were performed using the ligand poses derived from docking as starting points. The MD simulations confirm hypotheses derived from docking. Initial ligand orientations remained stable. Furthermore, a dynamic view on receptor-ligand interactions could be elucidated. Interestingly, we found the orthosteric building block to control the orientation of the allosteric part of the molecules [99]. Whereas Atropine-based hybrid ligands showed strong allosteric interactions with EL3, the Scopolamine-based compounds were mainly oriented towards EL2. The reason for these different binding modes was found in a varying orientation of the orthosteric building block. The tropane moiety of Scopolamine (**4**) was flipped by approximately 180 degrees when compared with Atropine (**3**). This was caused by the space requirements of the epoxide group and the possibility to form a hydrogen bond with C429. The different orientation of the tropane ring system controls the binding mode of the allosteric building block. These findings are supported by mutational studies that show the dependency of dualsteric binding on the key residues $M_2$ Y177 and $M_2$ W422. Whereas ligand binding of Atropine-based structures is strongly decreased by the mutation $M_2$ W422A it is nearly unaffected by $M_2$ Y177A. On the other hand, the binding of Scopolamine-based hybrid structures was affected more by $M_2$ Y177A than by the mutation $M_2$ W422A.

One main goal of this study was to unveil how the activity of GPCRs could be fine-tuned in a ligand-dependent manner. Therefore, dualsteric ligands were investigated in terms of subtype selectivity, partial agonism and biased signaling.

Several dualsteric ligands, such as Atr-6-naph (**11**) and Iper-6-phth (**15**), showed a strong preference for the $M_2$ AChR over $M_5$ AChR. Binding mode investigations on the basis of structural models led to an explanation of the reported subtype selectivity [36]. Residues that contribute to allosteric modulation are located in the EL2 and in the EL3. Receptor-ligand interactions to both extracellular loops can enhance ligand binding as reported for dualsteric ligands. Atr-6-naph (**11**) as well as Iper-6-phth (**15**) shows interactions to both extracellular loops in the $M_2$ AChR. These required interactions that build a connection between EL2 and EL3 were missing in the $M_5$ AChR. This result encourages focusing on the allosteric binding site for the development of subtype-selective ligands.

Several dualsteric agonists were shown to have more than one binding mode. The resulting coexistence of two functionally distinct receptor populations that are stabilized by one ligand represents a novel concept for partial agonism that is called *dynamic ligand binding* [105]. This study illustrates different involved binding modes: The dualsteric binding pose stabilizes active receptor conformations and therefore contributes to the agonistic properties of the ligand. On the other hand, the purely allosteric binding mode allows for the stabilization of inactive receptor states and shows opposite effects on receptor activation. Hence, the amount of activation depends on the fractional receptor occupancy. A higher tendency of a ligand to bind in the dualsteric mode would increase its agonistic property. But then preferred allosteric binding would lead to decreasing efficacy and therefore to partial agonism. Docking experiments in combination with MD simulations and subsequent 3D-pharmacophore analyses led to a rationalization of structure activity relationship. The length of the aliphatic carbon chain plays a highly important role: While Iper-8-naph (**17**) is a full agonist that binds in a dualsteric way, Iper-6-naph (**16**) and Isox-6-naph (**14**) become partial agonists due to their ability to bind allosterically as well. The isoxazole in Isox-6-naph (**14**) forms an intramolecular π-π-interaction, which stabilizes a conformation that prefers the allosteric binding mode. Hence, Isox-6-naph (**14**) is a partial agonist with low efficacy. Iper-6-naph (**16**) is unable to form a π-π-interaction like Isox-6-naph (**14**). Therefore Iper-6-naph (**16**) shows a higher preference for the dualsteric binding mode but lower than Iper-8-naph (**17**), which turns Iper-6-naph (**16**) into a partial agonist with higher efficacy than Isox-6-naph (**14**).

GPCRs trigger multiple intracellular mechanisms, which make them highly complex signaling machineries. The modulation of GPCRs in a ligand-dependent manner that leads to the activation of a distinct signaling pathway offers plenty of clinical benefits. The general model of GPCR activation is characterized by a movement of the transmembrane domains. The intracellular site opens and thereby reveals epitopes for the binding of signaling proteins. This movement goes along with a constriction of the extracellular region. As shown by the homology models, the preferably $G_i$ coupled even-numbered MAChRs indicate a wider allosteric vestibule than the odd-numbered. It could be shown that the distance between $M_2$ Y177 and $M_2$ W422 (and corresponding residues) can be used as a structural descriptor: A higher distance is correlated with a preference for the coupling of $G_i$ proteins. Docking in combination with MD simulations showed that dualsteric ligands can hamper the extracellular rearrangement, which leads to biased signaling. Simulations of $M_2$ AChR in complex with Iperoxo (**5**) confirm the strong constriction of the extracellular side. In contrast to the superagonist Iperoxo (**5**), the dualsteric ligands Iper-6-naph (**16**) and Iper-8-naph (**17**) hinder the closure of the allosteric binding pocket. Due to the longer chain length of Iper-8-naph (**17**), the allosteric building block sticks out of the allosteric pocked. Our models describe this effect by hindrance of the allosteric rearrangement upon activation, which explains the experimentally described slight $G_i$ bias (1.8 fold preference for $G_i$ [105]). Similarly, Iper-6-naph (**16**) shows a 10 fold higher $G_i$ bias than Iper-8-naph (**17**) [105], which could be mechanistically explained by the shorter aliphatic chain leading to a deeper binding location of the allosteric building block. Hence the big rigid ring system located between $M_2$ Y177 and $M_2$ W422 is able to hamper the constriction of the extracellular region to a larger extent than Iper-8-naph (**17**).

Taken together, dualsteric ligand binding provides plenty of possibilities to modulate the receptor function in a predictable way. This includes subtype selectivity, partial agonism and biased signaling. Allosteric binding properties can be influenced by variation of the orthosteric building block. The usage of a different chain length and variable allosteric building blocks enables medicinal chemists to design specific ligands with a desired modulation of GPCR functions.

# 6 Conclusion and outlook

GPCRs enable the transmission of signals into cells, which is essential for the regulation of biological systems. They represent integrative and highly dynamic signaling machines that recognize extracellular stimuli, adapt their conformation and hence allow for an intracellular response. Therefore GPCRs are highly interesting drug targets with a broad range of clinical applications. This study aimed at an elucidation of GPCR function on a molecular level. The knowledge of activation mechanisms and the resulting conformational changes is crucial for the rational design of specific ligands. Due to available crystal structures and experimental data, MAChR are classic examples to study GPCR functions.

In this study, we successfully developed structural models for all five MAChR subtypes in both the inactive and an active-like receptor state. These models unveiled structural characteristics that provide a deeper understanding of this protein class and indicated structural requirements for ligand binding.

Docking, MD simulations and 3D-pharmacophore modeling were combined to prove the concept of dualsteric ligand binding on a structural level. The investigated ligands were shown to bind simultaneously to the orthosteric and the allosteric binding site. This unconventional binding mode offers the possibility to fine-tune the receptor function. Whereas purely orthosteric (or purely allosteric) ligands stabilize a larger ensemble of receptor conformations, dualsteric ligands can stabilize more specific receptor states.

We reached our goal to explain experimentally determined ligand-dependent receptor modulation by dualsteric ligands. Allosteric epitopes on the extracellular side allow for subtype selective binding. We showed that orthosteric building blocks control the accessibility of these epitopes by allosteric moieties and thereby control subtype selectivity.

Further, we explored and mechanistically explained a novel concept for partial agonism, called *dynamic ligand binding*. We verified the co-existence of two functionally different populations of receptor-ligand complexes (inactive and active). Variations of the ligand structure provide the possibility to pharmacologically balance between these two functional states, which leads to partial agonists with predictable efficacy.

Due to the multiple signaling functions of GPCRs, it would be desirable to activate a distinct intracellular pathway upon ligand binding. Our dynamic model nicely illustrates how dualsteric ligands hamper the rearrangement of the allosteric binding site. This results in a restriction of the whole signaling repertoire and leads to functional selectivity with a strong $G_i$ bias.

Taken together, this study provides the structural basis for understanding specific modulation of MAChRs with respect to ligand design. This includes subtype selectivity, partial agonism and biased signaling. Our dynamic structural models show high explanatory power and can therefore be used as starting point for the rational design of specific GPCR modulators.

# 7 Experimental section

This thesis mainly uses *in silico* tools for the development of computational models. Methods and algorithms are described in chapter 3. This experimental section contains details about the parameters used for conducting computational experiments.

## 7.1 Homology modeling

The sequence alignment of the five investigated MAChRs was performed by the web tool ClustalW [107] using the following UniProt-entries: P11229 ($M_1$ AChR), P08172 ($M_2$ AChR), P20309 ($M_3$ AChR), P08173 ($M_4$ AChR), P08912 ($M_5$ AChR) [108]. On this basis a phylogenetic analysis was carried out with ETE [109]. The crystal structure of the inactive $M_2$AChR (PDB: 3UON) [94] was used as template for the inactive $M_4$AChR model. $M_1$AChR and $M_5$AChR were built on the basis of the inactive $M_3$AChR crystal structure (PDB: 4DAJ) [95]. All active-conformation receptor models were obtained from the active-like crystal structure of $M_2$AChR (PDB: 4MQS) [32]. The MAChR homology models were obtained by using the homology modeling tool from MOE (*Molecular Operating Environment (MOE)*, 2014.09; Chemical Computing Group Inc.). Initially 10 main chain models were built, each of them with 3 side chain samples. The temperature was set on 300 K and the OPLS-AA force field [110] was chosen. This results in 30 intermediate models with an RMS gradient of 1. Out of these 30 intermediate models, the final homology models were built by applying refinement protocols with an RMS gradient of 0.5. Subsequently, side chain positions were refined to optimize the protein geometry taking into account typical dihedral angle distributions. For further structural refinement, short MD simulations (10 ns) of the homology models were carried out.

## 7.2 Docking

All docking experiments described in this study were carried out with the CCDCs software GOLD 5.1 [76]. Prior to the docking experiments the ligand conformations were generated by Corina [111]. The preparation of protein structures was done with the modeling suite MOE (*Molecular Operating Environment (MOE)*, 2014.09; Chemical Computing Group Inc.). All ligands and water molecules were removed and the right protonation states were assigned. The co-crystallized ligands QNB (**1**), Tiotropium (**2**) and Iperoxo (**5**) served as reference ligands for the docking experiments. All residues of the inner core region and the extracellular domains were defined as potential binding site. Default settings were used for ligand docking and GoldScore served as scoring function. The obtained docking poses and receptor-ligand interactions were analyzed with the software LigandScout 3.1 [88, 90] using a 3D-pharmacophore approach.

## 7.3 Molecular dynamics simulations

Desmond 3.2 [86] was applied for all MD simulations described in this study. An orthorhombic box was used to build the model systems with periodic boundary conditions in a NPT ensemble. The system temperature was kept at 300 K and the pressure at atmospheric pressure. The definition of transmembrane regions was taken from the OPM-database [112]. The receptor structures were embedded in a pre-equilibrated POPC-membrane (palmitoyl-oleoyl-phosphatidyl-choline bilayer) and solvated with SPC water and 0.15 M NaCl. All other parameters were set on default values. Each simulation consisted of an equilibration run of 6.92 ns followed by a production run (10 ns - 50 ns). Energy values were recorded every 1.2 ps and frames every 4.8 ps. The simulations were carried out on the Soroban computer cluster (Freie Universität Berlin) by using 24 CPUs. The obtained trajectories were analyzed with the software VMD [113]. The root mean square deviation was calculated for backbone heavy atoms from the initial protein conformations.

# 8 Summary

GPCRs represent one of the most important drug target families. They enable the transmission of signals into cells, which is crucial for the regulation of biological systems. GPCRs can recognize extracellular stimuli, adapt their conformation and hence allow for an intracellular response. This study shed light on the first two steps of GPCR function: ligand binding and the resulting conformational changes. Taking MAChR as representative example we clarified the specific receptor modulation by dualsteric ligands.

In this study, we successfully combined state-of-the-art modeling techniques to obtain structural and functional models with high explanatory power. These models comprise both inactive and active-like receptor states. After a characterization of the orthosteric binding side, we focused on *dualsteric ligand binding*. These kind of ligands bind simultaneously to the orthosteric and the allosteric binding site. This approach combines the high affinity of orthosteric ligands with the high specificity of the allosteric binding site.

Here we report the structural basis for a specific modulation of MAChRs by dualsteric ligand binding. This includes subtype selectivity, partial agonism and biased signaling. Our dynamic models illustrate how conformational changes can be triggered in a ligand-dependent manner. This offers the possibility to rationally design specific modulators for MAChRs but also for other GPCRs.

# 9 Zusammenfassung

G-Protein gekoppelte Rezeptoren (GPCRs) repräsentieren eine der wichtigsten Targetklassen für Arzneistoffe – mehr als 30% aller Medikamente addressieren GPCR-vermittelte Mechanismen. Als Transmembranproteine stellen diese Rezeptoren eine Verbindung des Zellinneren mit der Umgebung her und sind so an zahlreichen essentiellen Regulationsmechanismen beteiligt. Auf mechanistischer Ebene führen extrazelluläre Ereignisse zu spezifischen Konformationsänderungen des Rezeptors und erzeugen so eine intrazelluläre Antwort. Die erst kürzlich verfügbaren Kristallstrukturen vieler GPCRs geben zwar einen Einblick in bestimmte Konformationen dieser Rezeptorfamilie, das dynamische Verständnis der Signalübertragung durch Konformationsänderungen des Rezeptors bleibt aber eine Herausforderung. In dieser Arbeit wurden extrazelluläre Ligandenbindungs-mechanismen und die daraus resultierenden Konformationsänderungen des Rezeptors mechanistisch untersucht und dynamisch modelliert. Besonderes Augenmerk lag dabei auf der spezifischen Rezeptormodulation durch dualsterische Liganden, einem neuen Konzept zur spezifischen und gleichzeitig effektiven Modulation von GPCRs. Muskarinische Acetylcholinrezeptoren wurden als Modell-system verwendet.

Durch die Kombination verschiedener computergestützter Methoden, wie Docking, 3D Pharmakophormodellierung, Homologiemodellierung und umfangreichen Molekulardynamiksimulationen konnten strukturell-mechanistische Rezeptormodelle erstellt werden. Diese Modelle bilden sowohl aktive als auch inaktive Rezeptorkonformationen ab und ermöglichen so eine differenzierte Beschreibung von Ligandeneffekten. Insbesondere die Rezeptormodulation durch dualsterische Liganden, die gleichzeitig an der orthosterischen und an allosterischen Region des Rezeptors binden, konnte erkärt werden. Die grundsätzliche Idee, dass die hohe Affinität orthosterischer Liganden mit spezifischen Effekten allostericher Liganden durch einfache Kombination mit einem Linker kombiniert werden kann, führt meist, aber nicht immer zum gewünschten Effekt. Unerwartetes Signalverhalten dualsterischer Liganden konnte durch unseren dynamischen Modellierungsansatz differenziert und mechanistisch erklärt werden.

Die hier vorgestellten Modelling-Untersuchungen an muskarinischen Acetylcholin-rezeptoren bilden die Vorraussetzungen für das Design spezifischer Rezeptor-modulation auf molekularer Ebene. Spezielle, sonst schwer erklärbare Effekte wie Subtyp-Selektivität, Partialagonismus und funktionelle Selektivität ('biased signalling') konnten mechanistisch abgebildet werden. Unsere dynamischen Rezeptormodelle erklären spezifische ligandeninduzierte Konformationsänderungen und die dadurch ausgelöste Signaltransduktion auf rationaler Ebene. Diese Erkenntnisse können direkt für das zielgerichtete Design von Wirkstoffen verwendet werden und potenziell auch auf andere G-Protein-gekoppelte Rezeptoren übertragen werden.

# 10 References


1. Bermudez, M. and G. Wolber, *Structure versus function—The impact of computational methods on the discovery of specific GPCR–ligands.* Bioorg. Med. Chem., 2015. e-pub ahead of print.

2. Horn, F., et al., *GPCRDB: an information system for G protein-coupled receptors.* Nucleic Acids Res., 1998. 26(1).

3. Gloriam, D.E., R. Fredriksson, and H.B. Schioth, *The G protein-coupled receptor subset of the rat genome.* BMC Genomics, 2007. 8(338).

4. Kolakowski, L.F., *GCRDb: a G-protein-coupled receptor database.* Recept. Channels, 1994. 2(1).

5. Bockaert, J. and J.P. Pin, *Molecular tinkering of G protein-coupled receptors: an evolutionary success.* EMBO J., 1999. 18(7).

6. Fredriksson, R., et al., *The G-protein-coupled receptors in the human genome form five main families. Phylogenetic analysis, paralogon groups, and fingerprints.* Mol. Pharmacol., 2003. 63(6).

7. Lagerstrom, M.C. and H.B. Schioth, *Structural diversity of G protein-coupled receptors and significance for drug discovery.* Nat. Rev. Drug Discovery, 2008. 7(4).

8. Schioth, H.B. and R. Fredriksson, *The GRAFS classification system of G-protein coupled receptors in comparative perspective.* Gen. Comp. Endocrinol., 2005. 142(1-2).

9. Mohr, K., et al., *Molecular alliance - from orthosteric and allosteric ligands to dualsteric/bitopic agonists at G protein coupled receptors.* Angew. Chem., Int. Ed., 2013. 52(2).

10. Milligan, G., *Constitutive activity and inverse agonists of G protein-coupled receptors: a current perspective.* Mol. Pharmacol., 2003. 64(6).

11. Kolb, P. and G. Klebe, *The golden age of GPCR structural biology: any impact on drug design?* Angew. Chem., Int. Ed., 2011. 50(49).

12. De Amici, M., et al., *Allosteric ligands for G protein-coupled receptors: A novel strategy with attractive therapeutic opportunities.* Med. Res. Rev., 2010. 30(3).

13. Schrage, R., et al., *Agonists with supraphysiological efficacy at the muscarinic M2 ACh receptor.* Br. J. Pharmacol., 2013. 169(2).

14. Wootten, D., A. Christopoulos, and P.M. Sexton, *Emerging paradigms in GPCR allostery: implications for drug discovery.* Nat. Rev. Drug Discovery, 2013. 12(8).

15. Bock, A. and K. Mohr, *Dualsteric GPCR targeting and functional selectivity: the paradigmatic M(2) muscarinic acetylcholine receptor.* Drug Discovery Today: Technol., 2013. 10(2).

16. Bock, A., et al., *Pilot the pulse: controlling the multiplicity of receptor dynamics.* Trends Pharmacol. Sci., 2014. 35(12).

17. Lefkowitz, R.J., *Seven transmembrane receptors - A brief personal retrospective.* Biochim. Biophys. Acta, Biomembr., 2007. 1768(4).

18. Peeters, M.C., et al., *Importance of the extracellular loops in G protein-coupled receptors for ligand recognition and receptor activation.* Trends Pharmacol. Sci., 2011. 32(1).

19. Salon, J.A., D.T. Lodowski, and K. Palczewski, *The significance of g protein-coupled receptor crystallography for drug discovery.* Pharmacol. Rev., 2011. 63(4).

20. Leschner, J., et al., *Interruption of the ionic lock in the bradykinin B2 receptor results in constitutive internalization and turns several antagonists into strong agonists.* J. Pharmacol. Exp. Ther., 2013. 344(1).

21. Nygaard, R., et al., *Ligand binding and micro-switches in 7TM receptor structures.* Trends Pharmacol. Sci., 2009. 30(5).

22. Trzaskowski, B., et al., *Action of molecular switches in GPCRs - theoretical and experimental studies.* Curr. Med. Chem., 2012. 19(8).

23. Isberg, V., et al., *GPCRDB: an information system for G protein-coupled receptors.* Nucleic Acids Res., 2014. 42(D1).

24. Deupi, X. and B. Kobilka, *Activation of G Protein Coupled Receptors*, in *Mechanisms and Pathways of Heterotrimeric G Protein Signaling*, S.S. R., Editor. 2007, Elsevier: Advances in Protein Chemistry.

25. Palczewski, K., et al., *Crystal structure of rhodopsin: A G protein-coupled receptor.* Science, 2000. 289(5480).

26. Katritch, V., V. Cherezov, and R.C. Stevens, *Structure-function of the G protein-coupled receptor superfamily.* Annu. Rev. Pharmacol. Toxicol., 2013. 53.

27. Shonberg, J., et al., *GPCR crystal structures: Medicinal chemistry in the pocket.* Bioorg. Med. Chem., 2015. e-pub ahead of print .

28. Warne, T., et al., *Structure of a beta(1)-adrenergic G-protein-coupled receptor.* Nature, 2008. 454(7203).

29. Rosenbaum, D.M., et al., *Structure and function of an irreversible agonist-beta(2) adrenoceptor complex.* Nature, 2011. 469(7329).

30. Rasmussen, S.G.F., et al., *Structure of a nanobody-stabilized active state of the beta(2) adrenoceptor.* Nature, 2011. 469(7329).

31. Scheerer, P., et al., *Crystal structure of opsin in its G-protein-interacting conformation.* Nature, 2008. 455(7212).

32. Kruse, A.C., et al., *Activation and allosteric modulation of a muscarinic acetylcholine receptor.* Nature, 2013. 504(7478).

33. Jacoby, E., et al., *The 7TM G-protein-coupled receptor target family.* ChemMedChem, 2006. 1(8).

34. Marinissen, M.J. and J.S. Gutkind, *G-protein-coupled receptors and signaling networks: emerging paradigms.* Trends Pharmacol. Sci., 2001. 22(7).

35. Klabunde, T. and G. Hessler, *Drug design strategies for targeting G-protein-coupled receptors.* ChemBioChem, 2002. 3(10).

36. Bermudez, M., C. Rakers, and G. Wolber, *Structural characteristics of the allosteric binding site represent a key to subtype selective modulators of muscarinic acetylcholine receptors.* Mol. Inf., 2015 accepted manuscript (in print).

37. Davie, B.J., A. Christopoulos, and P.J. Scammells, *Development of M-1 mAChR Allosteric and Bitopic Ligands: Prospective Therapeutics for the Treatment of Cognitive Deficits.* ACS Chem. Neurosci., 2013. 4(7).

38. Deupi, X., X.-D. Li, and G.F.X. Schertler, *Ligands stabilize specific GPCR conformations: but how?* Structure, 2012. 20(8).

39. Di Pizio, A. and M.Y. Niv, *Computational studies of smell and taste receptors.* Isr. J. Chem., 2014. 54(8-9).

40. Overington, J.P., B. Al-Lazikani, and A.L. Hopkins, *Opinion - How many drug targets are there?* Nat. Rev. Drug Discovery, 2006. 5(12).

41. Insel, P.A., et al., *Impact of GPCRs in clinical medicine: Monogenic diseases, genetic variants and drug targets.* Biochim. Biophys. Acta, Biomembr., 2007. 1768(4).

42. Mushtaq, G., et al., *Status of acetylcholinesterase and butyrylcholinesterase in Alzheimer's disease and type 2 diabetes mellitus.* CNS Neurol. Disord.: Drug Targets, 2014. 13(8).

43. Regulski, M., et al., *Chemistry and pharmacology of Angiotensin-converting enzyme inhibitors.* Curr. Pharm. Des., 2015. 21(13).

44. Immadisetty, K. and J.D. Madura, *A Review of Monoamine Transporter-Ligand Interactions.* Curr. Comput.-Aided Drug Des., 2013. 9(4).

45. Kruse, A.C., et al., *Muscarinic receptors as model targets and antitargets for structure-based ligand discovery.* Mol. Pharmacol., 2013. 84(4).

46. Caulfield, M.P. and N.J.M. Birdsall, *International Union of Pharmacology. XVII. Classification of muscarinic acetylcholine receptors.* Pharmacol. Rev., 1998. 50(2).

47. Penttila, J., H. Scheinin, and E. Syvalahti, *Measurement of anticholinergic effects of psychotropic drugs in humans.* Pharmacopsychiatry, 2005. 38(5).

48. Levay, M., et al., *NSC23766, a widely used inhibitor of Rac1 activation, additionally acts as a competitive antagonist at muscarinic acetylcholine receptors.* J. Pharmacol. Exp. Ther., 2013. 347(1).

49. Ozbilen, M., C.E. Adams, and J. Marley, *Anticholinergic effects of oral antipsychotic drugs of typicals versus atypicals over medium- and long-term: systematic review and meta-analysis.* Curr. Med. Chem., 2012. 19(30).

50. Rita, P. and D. Animesh, *An updated overview on Atropa belladonna L.* Int. Res. J. Pharm., 2011. 2(11).

51. Duncan, G. and D.J. Collison, *Role of the non-neuronal cholinergic system in the eye: A review.* Life Sci., 2003. 72(18-19).

52. Moulton, B.C. and A.D. Fryer, *Muscarinic receptor antagonists, from folklore to pharmacology; finding drugs that actually work in asthma and COPD.* Br. J. Pharmacol., 2011. 163(1).

53. Buels, K.S. and A.D. Fryer, *Muscarinic receptor antagonists: effects on pulmonary function*, in *Muscarinic Receptors*, A.D. Fryer, A. Christopoulos, and N.M. Nathanson, Editors. 2012, Springer: Handb. Exp. Pharmacol.

54. Kruse, A.C., et al., *Muscarinic acetylcholine receptor X-ray structures: potential implications for drug development.* Curr. Opin. Pharmacol., 2014. 16(C).

55. Harvey, R.D., *Muscarinic receptor agonists and antagonists: effects on cardiovascular function*, in *Muscarinic Receptors*, A.D. Fryer, A. Christopoulos, and N.M. Nathanson, Editors. 2012, Springer: Handb. Exp. Pharmacol.

56. Michel, M.C., *Therapeutic modulation of urinary bladder function: multiple targets at multiple levels.* Annu. Rev. Pharmacol. Toxicol., 2015. 55.

57. Iijima, K., S. De Wachter, and J.-J. Wyndaele, *Effects of the M3 receptor selective muscarinic antagonist darifenacin on bladder afferent activity of the rat pelvic nerve.* Eur. Urol., 2007. 52(3).

58. Langmead, C.J., J. Watson, and C. Reavill, *Muscarinic acetylcholine receptors as CNS drug targets.* Pharmacol. Ther., 2008. 117(2).

59. Eglen, R.M., A. Choppin, and N. Watson, *Therapeutic opportunities from muscarinic receptor research.* Trends Pharmacol. Sci., 2001. 22(8).

60. Dencker, D., et al., *Muscarinic acetylcholine receptor subtypes as potential drug targets for the treatment of schizophrenia, drug abuse, and Parkinson's disease.* ACS Chem. Neurosci., 2012. 3(2).

61. Birks, J., *Cholinesterase inhibitors for Alzheimer's disease.* Cochrane Database of Systematic Reviews, 2006. 1.

62. Kruse, A.C., et al., *Muscarinic acetylcholine receptors: novel opportunities for drug development.* Nat. Rev. Drug Discovery, 2014. 13(7).

63. Tytgat, G.N., *Hyoscine butylbromide - A review of its use in the treatment of abdominal cramping and pain.* Drugs, 2007. 67(9).

64. Sliwoski, G., et al., *Computational methods in drug discovery.* Pharmacol. Rev., 2014. 66(1).

65. Hawkins, P.C.D., A.G. Skillman, and A. Nicholls, *Comparison of shape-matching and docking as virtual screening tools.* J. Med. Chem., 2007. 50(1).

66. Costanzi, S., *Homology modeling of class a G protein-coupled receptors*, in *Homology Modeling*, A.J.W. Orry and R. Abagyan, Editors. 2012, Springer: Methods in molecular biology.

67. Saxena, A., R.S. Sangwan, and S. Mishra, *Fundamentals of homology modeling steps and comparison among important bioinformatics tools: an overview.* Sci. Int., 2013. 1(7).

68. Kalyaanamoorthy, S. and Y.-P.P. Chen, *Structure-based drug design to augment hit discovery.* Drug Discovery Today, 2011. 16(17-18).

69. Warren, G.L., et al., *A critical assessment of docking programs and scoring functions.* J. Med. Chem., 2006. 49(20).

70. Guedes, I.A., C.S. de Magalhães, and L.E. Dardenne, *Receptor–ligand molecular docking.* Biophys. Rev., 2014. 6(1).

71. Murgueitio, M.S., et al., *In silico virtual screening approaches for anti-viral drug discovery.* Drug Discovery Today: Technol., 2012. 9(3).

72. Morris, G.M., et al., *AutoDock4 and AutoDockTools4: Automated docking with selective receptor flexibility.* J. Comput. Chem., 2009. 30(16).

73. Ewing, T.J.A., et al., *DOCK 4.0: Search strategies for automated molecular docking of flexible molecule databases.* J. Comput.-Aided Mol. Des., 2001. 15(5).

74. Kamper, A., et al., *Fully automated flexible docking of ligands into flexible synthetic receptors using forward and inverse docking strategies.* J. Chem. Inf. Model., 2006. 46(2).

75. Friesner, R.A., et al., *Extra precision glide: Docking and scoring incorporating a model of hydrophobic enclosure for protein-ligand complexes.* J. Med. Chem., 2006. 49(21).

76. Verdonk, M.L., et al., *Improved protein-ligand docking using GOLD.* Proteins: Struct., Funct., Genet., 2003. 52(4).

77. Meier, R., et al., *PARADOCKS: a framework for molecular docking with population-based metaheuristics.* J. Chem. Inf. Model., 2010. 50(5).

78. Jones, G., P. Willett, and R.C. Glen, *Molecular recognition of receptor sites using a genetic algorithm with a description of desolvation.* J. Mol. Biol., 1995. 245(1).

79. Jones, G., et al., *Development and validation of a genetic algorithm for flexible docking.* J. Mol. Biol., 1997. 267(3).

80. Mortier, J., et al., *The impact of molecular dynamics on drug design: applications for the characterization of ligand–macromolecule complexes.* Drug Discovery Today, 2015. e-pub ahead of print.

81. Dror, R.O., et al., *Biomolecular simulation: a computational microscope for molecular biology.* Annu. Rev. Biophys., 2012. 41.

82. Berendsen, H.J.C., D. Vanderspoel, and R. Vandrunen, *GROMACS - a message-passing parallel molecular dynamics implementation.* Comput. Phys. Commun., 1995. 91(1-3).

83. Brooks, B.R., et al., *CHARMM: The Biomolecular Simulation Program.* J. Comput. Chem., 2009. 30(10).

84. Case, D.A., et al., *The Amber biomolecular simulation programs.* J. Comput. Chem., 2005. 26(16).

85. Phillips, J.C., et al., *Scalable molecular dynamics with NAMD.* J. Comput. Chem., 2005. 26(16).

86. Bowers, K.J., et al. *Scalable algorithms for molecular dynamics simulations on commodity clusters*. in *Proceedings of the ACM/IEEE Conference on Supercomputing (SC06)*. 2006. Tampa, FL: IEEE.

87. Wermuth, G., et al., *Glossary of terms used in medicinal chemistry (IUPAC Recommendations 1998).* Pure Appl. Chem., 1998. 70(5).

88. Wolber, G. and T. Langer, *LigandScout: 3-d pharmacophores derived from protein-bound Ligands and their use as virtual screening filters.* J. Chem. Inf. Model., 2005. 45(1).

89. Horvath, D., *Pharmacophore-based virtual screening*, in *Chemoinformatics and Computational Chemical Biology*, J. Bajorath, Editor. 2011, Springer: Methods in Molecular Biology.

90. Wolber, G., A.A. Dornhofer, and T. Langer, *Efficient overlay of small organic molecules using 3D pharmacophores.* J. Comput.-Aided Mol. Des., 2006. 20(12).

91. Guner, O., O. Clement, and Y. Kurogi, *Pharmacophore modeling and three dimensional database searching for drug design using catalyst: Recent advances.* Curr. Med. Chem., 2004. 11(22).

92. Dixon, S.L., A.M. Smondyrev, and S.N. Rao, *PHASE: A novel approach to pharmacophore modeling and 3D database searching.* Chem. Biol. Drug Des., 2006. 67(5).

93. Labute, P., et al., *Flexible alignment of small molecules.* J. Med. Chem., 2001. 44(10).

94. Haga, K., et al., *Structure of the human M2 muscarinic acetylcholine receptor bound to an antagonist.* Nature, 2012. 482(7386).

95. Kruse, A.C., et al., *Structure and dynamics of the M3 muscarinic acetylcholine receptor.* Nature, 2012. 482(7386).

96. Ramachandran, G.N., C. Ramakrishnan, and V. Sasisekharan, *Stereochemistry of polypeptide chain configurations.* J. Mol. Biol., 1963. 7(1).

97. Duran, C.E., M. Azermai, and R.H. Vander Stichele, *Systematic review of anticholinergic risk scales in older adults.* Eur. J. Clin. Pharmacol., 2013. 69(7).

98. Bock, A., et al., *The allosteric vestibule of a seven transmembrane helical receptor controls G-protein coupling.* Nat. Commun., 2012. 3(1044).

99. Schmitz, J., et al., *Dualsteric muscarinic antagonists-orthosteric binding pose controls allosteric subtype selectivity.* J. Med. Chem., 2014. 57(15).

100. Leppik, R.A., et al., *Role of acidic amino acids in the allosteric modulation by gallamine of antagonist binding at the m2 muscarinic acetylcholine receptor.* Mol. Pharmacol., 1994. 45(5).

101. Antony, J., et al., *Dualsteric GPCR targeting: a novel route to binding and signaling pathway selectivity.* Faseb J., 2009. 23(2).

102. Holzgrabe, U. and K. Mohr, *Allosteric modulators of ligand binding to muscarinic acetylcholine receptors.* Drug Discovery Today, 1998. 3(5).

103. Jaeger, D., et al., *Allosteric small molecules unveil a role of an extracellular E2/transmembrane helix 7 junction for G protein-coupled receptor activation.* J. Biol. Chem., 2007. 282(48).

104. Bruning, J.B., et al., *Coupling of receptor conformation and ligand orientation determine graded activity.* Nat. Chem. Biol., 2010. 6(11).

105. Bock, A., et al., *Dynamic ligand binding dictates partial agonism at a G protein-coupled receptor.* Nat. Chem. Biol., 2014. 10(1).

106. Dror, R.O., et al., *Structural basis for modulation of a G-protein-coupled receptor by allosteric drugs.* Nature, 2013. 503(7475).

107. Larkin, M.A., et al., *Clustal W and clustal X version 2.0.* Bioinformatics, 2007. 23(21).

108. Bateman, A., et al., *UniProt: a hub for protein information.* Nucleic Acids Res., 2015. 43(D1).

109. Huerta-Cepas, J., J. Dopazo, and T. Gabaldon, *ETE: a python environment for tree exploration.* BMC Bioinf., 2010. 11(24).

110. Jorgensen, W.L., D.S. Maxwell, and J. TiradoRives, *Development and testing of the OPLS all-atom force field on conformational energetics and properties of organic liquids.* J. Am. Chem. Soc., 1996. 118(45).

111. Sadowski, J., J. Gasteiger, and G. Klebe, *Comparison of automatic three-dimensional model builders using 639 X-ray structures.* J. Chem. Inf. Comput. Sci., 1994. 34(4).

112. Lomize, M.A., et al., *OPM: Orientations of proteins in membranes database.* Bioinformatics, 2006. 22(5).

113. Humphrey, W., A. Dalke, and K. Schulten, *VMD: Visual molecular dynamics.* J. Mol. Graphics Modell., 1996. 14(1).

# List of Figures

# List of Tables

# Curriculum vitae

# Publications

## Peer-reviewed articles


1. Bermudez, M., et al., Structural characteristics of the allosteric binding site represent a key to subtype selective modulators of muscarinic acetylcholine receptors, *Mol Inf*, accepted manuscript (in print), 2015.

2. Bermudez, M. and G. Wolber, Structure versus function—The impact of computational methods on the discovery of specific GPCR–ligands, *Bioorg Med Chem*, e-pub ahead of print, 2015.

3. Mortier, J., et al., The impact of molecular dynamics on drug design: applications for the characterization of ligand–macromolecule complexes, *Drug Discov Today*, e-pub ahead of print, 2015.

4. Schmitz, J., et al., Dualsteric muscarinic antagonists - orthosteric binding pose controls allosteric subtype selectivity, *J Med Chem*, 2014. 57(15).

5. Levay, M., et al., NSC23766, a widely used inhibitor of Rac1 activation, additionally acts as a competitive antagonist at muscarinic acetylcholine receptors, *J Pharmacol Exp Ther*, 2013. 347(1).

6. Leschner, J., et al., Interruption of the Ionic Lock in the Bradykinin B-2 Receptor Results in Constitutive Internalization and Turns Several Antagonists into Strong Agonists, *J Pharmacol Exp Ther*, 2013. 344(1).

7. Murgueitio, M.S., et al., In silico virtual screening approaches for anti-viral drug discovery, *Drug Discov Today Technol*, 2012. 9(3).

8. Faussner, A., et al., Binding characteristics of 3H -JSM10292: a new cell membrane-permeant non-peptide bradykinin B2 receptor antagonist, *Br J Pharmacol*, 2012. 167(4)

## Conference proceedings

1. Oral presentation: Bermudez M, Wolber G. Modulation of GPCR signaling: Understanding ligand binding effects. DPhG Annual meeting 2014 Frankfurt(Main), Germany; September 24-26, 2014.

2. Poster: Bermudez M, Wolber G. Structural comparison of the allosteric binding pocket in muscarinic acetylcholine receptors. DPhG Annual meeting 2014, Frankfurt(Main), Germany; September 24-26, 2014.

3. Oral presentation: Bermudez M, Wolber G. Novel bradykinin B2 receptor antagonists identified by virtual screening. 248th National Meeting of the American Chemical Society, San Francisco, USA; August 10-14, 2014.

4. Poster: Bermudez M, Wolber G. Molecular modeling of subtype selective muscarinic antagonists. 248th National Meeting of the American Chemical Society, San Francisco, USA; August 10-14, 2014.

5. Poster: Bermudez M, Wolber G., Dualsteric muscarinic antagonists – orthosteric binding pose controls allosteric subtype-selectivity. Tag der Pharmazie 2014, Berlin, Germany; July 4, 2014.

6. Poster: Bermudez M, Wolber G. Dualsteric modulators of the M2 muscarinic acetylcholine receptor. 9th German Conference on Chemoinformatics 2013, Fulda, Germany; November 10-12, 2013.

7. Poster: Bermudez M, Wolber G. Rationalizing the binding mode of JSM10292. 2nd Berliner Chemie Symposium, Berlin, Germany; April 3, 2012.

8. Poster: Bermudez M, Wolber G. Design of novel non-peptide bradykinin B2 receptor antagonists by structure-based virtual screening. DPhG Doktorandentagung 2012, Weimar, Germany; November 14-17, 2012.

9. Oral presentation: Bermudez M, Wolber G. Design of non-peptide bradykinin B2 receptor antagonists by structure-based virtual screening. Tag der Pharmazie 2012, Berlin, Germany; July 6, 2012.

10. Poster: Bermudez M, Wolber G. Design of non-peptide bradykinin B2 receptor antagonists by structure-based virtual screening. EuroQSAR 2012, Vienna, Austria; August 26-30, 2012.

11. Poster: Bermudez M, Wolber, G., A novel, potent bradykinin B2 receptor antagonist. EUROPIN Summer School Drug Design 2011, Vienna, Austria; September 11-16, 2011.